International Journal of Solids and Structures 000 (2018) 1–14

Contents lists available at ScienceDirect

International Journal of Solids and Structures

journal homepage: www.elsevier.com/locate/ijsolstr

Anisotropic fracture forming limit diagram considering non-directionality of the equi-biaxial fracture strain

Namsu Park[a], Hoon Huh[a,*], Jeong Whan Yoon[a,b]

[a] School of Mechanical, Aerospace and Systems Engineering, KAIST, 291 Daehak-ro, Yuseong-gu, Daejeon 34141, Republic of Korea
[b] School of Engineering, Deakin University, Geelong Waurn Ponds, Victoria 3220, Australia

ARTICLE INFO

Article history:
Revised 1 May 2017
Available online xxx

Keyword:
Anisotropy
Ductile fracture criterion
Fracture forming limit diagram (FFLD)
Non-directionality
Sheet metal forming

ABSTRACT

This paper is concerned with modeling of anisotropic fracture forming limit diagram considering non-directionality of the equi-biaxial fracture strain. A new anisotropic ductile fracture criterion is developed based on the Lou–Huh ductile fracture criterion (Lou et al., 2012). In an attempt to predict the forming severity of advanced high-strength steel (AHSS) sheets, the proposed fracture criterion is converted into a Fracture Forming Limit Diagram (FFLD) and anisotropic fracture locus considering the sheet metal orientation. Tensile tests of the DP980 steel sheet with the thickness of 1.2 mm are conducted using various specimen geometries including pure shear, dog-bone, and flat grooved specimens. With Digital Image Correlation (DIC) method, equivalent plastic strain distribution on the specimen surface is computed until surface crack initiates. The fracture predictability of the proposed fracture criterion is evaluated with the experimental results which cover a wide range of stress states in various loading directions. By comparing fracture strains obtained from the experiments with the ones predicted from the proposed fracture criterion, it is clearly confirmed that the fracture criterion proposed is capable of predicting the equivalent plastic strain at the onset of fracture with great accuracy over a wide range of stress states while keeping non-directionality of the equi-biaxial fracture strain.

© 2018 Published by Elsevier Ltd.

In the automotive industries, it is important to evaluate the forming severity of sheet metals to make an efficient design of structural components for the auto-body. In dealing with the forming severity, necking has been regarded as a major failure mechanism because it gives the direct information on the loss of a load carrying capability. Various analytical models based on necking, thus, have been proposed to evaluate the forming limit of sheet metals accurately: the Hill's localized necking model (Hill, 1952); the Swift's diffuse necking model (Swift, 1952); the imperfection-based Marciniak–Kuczynski model (Marciniak and Kuczynski, 1967); the modified maximum force criterion (Hora et al., 1996); and the vertex theory (Stören and Rice, 1975; Zhu et al., 2001). Meanwhile, the experimental method to measure the forming limit was firmly established in the 1960s by Keeler and Backofen (1964) and Goodwin (1968). This experimental methodology has been widely accepted as a standard tool and named as Forming Limit Diagram (FLD) for indicating the forming limit of sheet metals. The conventional FLD describes necking limits and thickness reductions in terms of the major and minor strains over the deformation modes from the uniaxial tension to the equi-biaxial tension.

With increasing demands of advanced high strength steels (AHSSs), aluminum alloys, and magnesium alloys to the automotive industry, there arises a challenging issue to deal with a sudden fracture of sheet metals during forming processes. This undesired failure mode, which is often called the shear fracture, mainly results from the low ductility of advanced metal sheets and it shows the fracture surface slanted along the maximum shear stress direction through the thickness of metal sheets with little amount of necking. This failure phenomenon is observed not only in tension but also in shear and compression conditions where the thickness reduction is negligible. It is, thus, challenging to predict the forming severity of advanced metal sheets appropriately using the conventional FLDs and various approaches based on necking or thinning.

The failure of advanced metals can be regarded as ductile fracture with some amount of deformation, which is induced by the mutual influence among nucleation, growth, and coalescence of micro-cavities or voids. The forming severity of advanced metal sheets, hence, can be evaluated in aid of ductile fracture criterion instead of necking-based forming limit criterion, which lies in the fact that the ductile fracture can take place over a wide range of

* Corresponding author.
E-mail address: hhuh@kaist.ac.kr (H. Huh).

https://doi.org/10.1016/j.ijsolstr.2018.01.009
0020-7683/© 2018 Published by Elsevier Ltd.

stress states including shear and compression conditions under low and negative stress triaxiality as reported by Bao and Wierzbicki (2004), Børvik et al. (2010), and Khan and Liu (2012a, b).

Various approaches on the ductile fracture have been proposed over the past decades to predict the onset of fracture over a wide range of stress states. The proposed approaches can be classified into two categories such as coupled and uncoupled fracture criteria. The main difference between these two categories of fracture criteria is whether the strength of metals is affected by damage accumulated through the void nucleation, the growth, and the coalescence of voids. Coupled fracture criteria are firmly established based on the postulate explained above; on the contrary, uncoupled fracture criteria do not consider the effect of accumulated damage on the load carrying capability of metals. In the case of coupled fracture criteria, the nucleation and the growth of voids are mathematically formulated based on porous plasticity introduced by Gurson (1977). This approach has gained great attention after Tvergaard and Needleman (1984) incorporated the effect of void coalescence, which is named as the Gurson–Tvergaard–Needleman (GTN) ductile fracture criterion. In the GTN ductile fracture criterion, the accumulated damage is represented by the void volume fraction which is coupled by the constitutive equation so as to induce the effect of strength weakening. As a base formula, the GTN ductile fracture criterion has been widely utilized to predict shear localization at the low stress triaxiality (Xue, 2008; Nahshon and Hutchinson, 2008; Nielsen and Tvergaard 2010) as well as void shape changes (Budiansky et al., 1982; Gologanu et al., 1993; Danas and Castaneda, 2012). Another popular coupled fracture criteria are based on the continuum damage mechanics (CDM) introduced by Kachanov (1958), which is further improved by various research works (Lemaitre, 1985, 1992, 2000; Chaboche, 1981, 1988a, 1988b; Saanouni and Chaboche, 2003; Brünig 2003a, 2003b, 2006, 2011). The CDM considers the damage as an internal variable which grows with plastic deformation to represent the local distribution of micro-defects which eventually induce the change of material properties such as macroscopic elastic and hardening modulus. In the case of uncoupled fracture criteria, dozens of approaches have been proposed based on microscopic mechanisms and experimental observations of the ductile fracture with various hypotheses to solve for special problems (Freudenthal, 1950; Cockcroft and Latham, 1968; Brozzo et al., 1972; Oh et al., 1979; Oyane et al., 1980; Clift et al., 1990; Ko et al., 2007; Xue and Wierzbicki, 2008; Bai and Wierzbicki, 2010; Lou et al., 2012, 2014; Park et al., 2015; Mohr and Marcadet, 2015). The uncoupled fracture criteria employ a scalar damage indicator, usually expressed in an integral form, which continually evolves with plastic deformation. In this case, the ductile fracture is known to initiate when the damage indicator reaches unity. By employing an uncoupled fracture criterion in the prediction of fracture initiation in aid of finite element analysis, Dunand and Mohr (2010) made great emphasis on the careful choice of hardening moduli in large plastic strain range in order to guarantee an accuracy of the fracture prediction. In an attempt to evaluate the anisotropy on the onset of fracture, Luo et al. (2012) introduced an uncoupled non-associated ductile fracture criterion based on the linear transformation of the strain tensor. Gu and Mohr (2015) formulated an anisotropic extension of the Hosford–Coulomb shear localization criterion based on the linear transformation of the stress tensor. In modeling anisotropic ductile fracture criteria above, linear transformation tensors play a key role in the construction of the anisotropic fracture configuration and the components of those transformation tensors were set as the model parameters to be calibrated. Recently, Park et al. (2017) proposed an uncoupled anisotropic ductile fracture criterion on the basis of the Lou–Huh ductile fracture criterion and suggested an anisotropic stress triaxiality based on the Hill's 48 criterion. In their research, various fracture-based forming limit criteria were proposed and discussed according to typical stress states along different orientations of the metal sheet.

The main concern of the present paper is to propose a generalized anisotropic fracture forming limit criterion for the advanced metal sheets considering non-directionality of the equi-biaxial fracture strain. The uncoupled anisotropic ductile fracture criterion by Park et al. (2017) is extended with a generalized anisotropic stress triaxiality based on the Yld91 criterion (Barlat et al., 1991) for the application to advanced metal sheets including aluminum alloys. A theoretical transformation procedure is introduced to construct the fracture forming limit diagram. Hydraulic bulge and tensile tests with various specimen geometries are carried out to evaluate the material properties and the equivalent plastic strains at the onset of fracture of the DP980 1.2t (DP980 with the thickness of 1.2 mm) steel sheet. With the postulate of a proportional loading condition, the parameters of the proposed fracture criterion are calibrated and the prediction of the fracture criterion is confirmed with the experimental results. Appendix A is also provided to generalize anisotropic triaxiality for Yld2004-18p criterion (Barlat et al., 2005).

2. Development of a new anisotropic ductile fracture criterion

2.1. Anisotropic stress triaxiality based on the Yld91 criterion

With the Lode parameter L_P or the normalized Lode angle $\bar{\theta}$, the stress triaxiality η_v plays a key role in modeling uncoupled ductile fracture criterion for the reason that the combination of these stress invariants represents the direction of three-dimensional principal stress vector $(\sigma_1,\sigma_2,\sigma_3)$ in Haigh–Westergaard space. It is, however, challenging to consider the directionality of typical stress states on the material orientation using these stress invariants because they are isotropic indicators. In an attempt to involve the influence of material anisotropy into the stress triaxiality, Park et al. (2017) suggested the anisotropic stress triaxiality based on the Hill's 48 criterion $\bar{\sigma}_H$ as follows:

$$\eta_H = \frac{\sigma_m}{\bar{\sigma}_H} = \frac{1}{3}\frac{\sigma_1+\sigma_2+\sigma_3}{\sqrt{(\sigma_1-\sigma_3)^2\left[Ff^2+Gg^2+Hh^2+2\left(Ll^2+Mm^2+Nn^2\right)\right]}}$$

$$\text{where } \sigma_m = \frac{\mathrm{tr}(\boldsymbol{\sigma})}{3} \tag{1}$$

$$f = \begin{bmatrix} \left(1-2x^2+x^4-2y^2+c^2x^4+2x^2y^2+2cx^2-2cx^4 \right. \\ \left. -4cx^2y^2+2c^2x^2y^2-2xyzs+2xyzsc\right) \\ +\left(\frac{1-L_P}{2}\right)\left(-c^2+2c^2y^2-2xyzs+2xyzsc\right) \\ +\left(\frac{1+L_P}{2}\right)\left(-x^2-y^2+2y^4+c^2x^2-c^2y^2+2c^2y^4+x^2y^2 \right. \\ \left. +4cy^2-4cy^4+c^2x^2y^2-2cx^2y^2\right) \end{bmatrix}$$

$$g = \begin{bmatrix} \left(x^2-2x^4+y^2+c^2x^2-2c^2x^4-c^2y^2-x^2y^2-4cx^2+4cx^4 \right. \\ \left. -c^2x^2y^2+2cx^2y^2\right) \\ +\left(\frac{1+L_P}{2}\right)\left(-1+2x^2+2y^2-y^4-c^2y^4-2x^2y^2-2cy^2 \right. \\ \left. +2cy^4-2c^2x^2y^2+4cx^2y^2-2xyzs+2xyzsc\right) \\ +\left(\frac{1-L_P}{2}\right)\left(-c^2+2c^2x^2+2xyzs-2xyzsc\right) \end{bmatrix}$$

$$h = \begin{bmatrix} \left(x^4-2c^2x^2+c^2x^4+2cx^2-2cx^4+2xyzs-2xyzsc\right) \\ +\left(\frac{1+L_P}{2}\right)\left(-y^4+2c^2y^2-c^2y^4-2cy^2+2cy^4 \right. \\ \left. +2xyzs-2xyzsc\right) \\ +\left(\frac{1-L_P}{2}\right)\left(-1+2c^2+x^2+y^2-c^2x^2-c^2y^2 \right. \\ \left. -x^2y^2-c^2x^2y^2+2cx^2y^2\right) \end{bmatrix}$$

$$l = \begin{bmatrix} \left(-xs - yz + x^3s + x^2yz - cx^3s + xy^2s - cxy^2s - 2cx^2yz \right. \\ \left. + c^2x^2yz\right) \\ + \left(\frac{1+L_P}{2}\right)\left(y^3z - 2cy^3z + c^2y^3z + cyz\right) \\ + \left(\frac{1-L_P}{2}\right)\left(c^2yz + csx + xy^2s - cxy^2s\right) \end{bmatrix}$$

$$m = \begin{bmatrix} \left(x^3z - 2cx^3z + c^2x^3z + cxz\right) \\ + \left(\frac{1+L_P}{2}\right)\left(ys - xz - y^3s + xy^2z + cy^3s - x^2ys + cx^2ys \right. \\ \left. - 2cxy^2z + c^2xy^2z\right) \\ + \left(\frac{1-L_P}{2}\right)\left(-c^2xz + cys + x^2ys - cx^2ys\right) \end{bmatrix}$$

$$n = \begin{bmatrix} \left(x^3y + cxy - c^2xy - 2cx^3y - x^2zs + c^2x^3y + cx^2zs\right) \\ + \left(\frac{1+L_P}{2}\right)\left(xy^3 + cxy - c^2xy - 2cxy^3 + y^2zs \right. \\ \left. + c^2xy^3 - cy^2zs\right) + \left(\frac{1-L}{2}\right)(-csz) \end{bmatrix},$$

$$L_P = \frac{2\sigma_2 - \sigma_1 - \sigma_3}{\sigma_1 - \sigma_3} \tag{2}$$

where $c = \cos\theta_r$, $s = \sin\theta_r$, $\hat{\mathbf{u}} = x\hat{\mathbf{i}} + y\hat{\mathbf{j}} + z\hat{\mathbf{k}}$ is a unit vector for a rotation axis and $\theta_r$is a rotation angle as shown in Fig.1.

Here, F, G, H, L, M, and N are the anisotropic parameters of the Hill's 48 criterion. This anisotropic stress triaxiality is able to deal with the material anisotropy on typical stress states in general three-dimensional space. Note that the anisotropic yield criterion to describe the anisotropic stress triaxiality have to include three-dimensional stress state in terms of the stress triaxiality, the Lode parameter, and the equivalent stress $(\eta_A, L_P, \bar{\sigma}_A)$. In the present paper, the anisotropic stress triaxiality is generalized based on the Yld91 criterion $\bar{\sigma}_A$ so as to extend the applicability of the anisotropic stress triaxiality to various materials including aluminum alloys.

$$2\bar{\sigma}_A^m = |S_2 - S_3|^m + |S_3 - S_1|^m + |S_1 - S_2|^m \tag{4}$$

$$\eta_A = \frac{\sigma_m}{\bar{\sigma}_A} = \frac{1}{3}\frac{\sigma_1 + \sigma_2 + \sigma_3}{\sqrt[m]{\frac{|S_2-S_3|^m + |S_3-S_1|^m + |S_1-S_2|^m}{2}}} \quad \text{where } \sigma_m = \frac{\mathrm{tr}(\boldsymbol{\sigma})}{3} \tag{5}$$

where S_1, S_2, and S_3 are the principal values of the isotropic plastic equivalent (IPE) transformed stress tensor $\mathbf{s}$, and the exponent m denotes an isotropic parameter that can assume any positive and real value greater than unity. In the Voigt notation, the IPE transformed stress vector $\tilde{\mathbf{s}}$ is defined as:

$$\tilde{\mathbf{s}} = \mathbf{L}\tilde{\sigma} = \begin{Bmatrix} s_{xx} \\ s_{yy} \\ s_{zz} \\ s_{yz} \\ s_{zx} \\ s_{xy} \end{Bmatrix} = \begin{bmatrix} (c_2+c_3)/3 & -c_3/3 & -c_2/3 & 0 & 0 & 0 \\ -c_3/3 & (c_3+c_1)/3 & -c_1/3 & 0 & 0 & 0 \\ -c_2/3 & -c_1/3 & (c_1+c_2)/3 & 0 & 0 & 0 \\ 0 & 0 & 0 & c_4 & 0 & 0 \\ 0 & 0 & 0 & 0 & c_5 & 0 \\ 0 & 0 & 0 & 0 & 0 & c_6 \end{bmatrix} \begin{Bmatrix} \sigma_{xx} \\ \sigma_{yy} \\ \sigma_{zz} \\ \sigma_{yz} \\ \sigma_{zx} \\ \sigma_{xy} \end{Bmatrix} \tag{6}$$

where $\mathbf{L}$ is the linear transformation operator proposed by Barlat et al. (1991) and c_i $(i = 1, \ldots, 6)$ are the parameters describing the anisotropy of the metallic material. In aid of tensor transformation based on the Rodrigues' rotation formula (Rodriguez, 1840) with the Lode parameter, the IPE transformed stress tensor $\mathbf{s}$ can be written as:

$$\mathbf{s} = (\sigma_1 - \sigma_3)\begin{bmatrix} \frac{c_3h - c_2g}{3} & c_6n & c_5m \\ c_6n & \frac{c_1f - c_3h}{3} & c_4l \\ c_5m & c_4l & \frac{c_2g - c_1f}{3} \end{bmatrix} = \begin{bmatrix} s_{xx} & s_{xy} & s_{xz} \\ s_{xy} & s_{yy} & s_{yz} \\ s_{xz} & s_{yz} & s_{zz} \end{bmatrix} \tag{7}$$

where f, g, h, l, m, and n are the sub-functions in Eq. (2). The principal values of the IPE transformed stress tensor $\mathbf{s}$ can be expressed by its invariants:

$$\begin{Bmatrix} S_1 \\ S_2 \\ S_3 \end{Bmatrix} = 2\sqrt{-Q}\begin{Bmatrix} \cos\left(\frac{\theta_A}{3}\right) \\ \cos\left(\frac{\theta_A - 2\pi}{3}\right) \\ \cos\left(\frac{\theta_A + 2\pi}{3}\right) \end{Bmatrix}$$

where

$$\theta_A = \cos^{-1}\left(\frac{R}{\sqrt{-Q^3}}\right), \quad Q = \frac{I_2}{3}, \quad R = \frac{I_3}{2}$$

$$I_2 = (\sigma_1 - \sigma_3)^2 \begin{bmatrix} \left(\frac{-c_2g+c_3h}{3}\right)\left(\frac{-c_3h+c_1f}{3}\right) + \left(\frac{-c_3h+c_1f}{3}\right)\left(\frac{-c_1f+c_2g}{3}\right) \\ + \left(\frac{-c_2g+c_3h}{3}\right)\left(\frac{-c_1f+c_2g}{3}\right) \\ - c_6^2n^2 - c_4^2l^2 - c_5^2m^2 \end{bmatrix}$$

$$I_3 = (\sigma_1 - \sigma_3)^3 \begin{bmatrix} \left(\frac{-c_2g+c_3h}{3}\right)\left(\frac{-c_3h+c_1f}{3}\right)\left(\frac{-c_1f+c_2g}{3}\right) + 2c_6^2n^2c_4^2l^2c_5^2m^2 \\ - \left(\frac{-c_2g+c_3h}{3}\right)c_4^2l^2 - \left(\frac{-c_3h+c_1f}{3}\right)c_5^2m^2 \\ - \left(\frac{-c_1f+c_2g}{3}\right)c_6^2n^2 \end{bmatrix} \tag{8}$$

where I_2 and I_3 are the second, and the third invariants of the IPE transformed stress tensor, $\mathbf{s}$, respectively. Note that the first invariant I_1 of the IPE transformed stress tensor, $\mathbf{s}$, is zero $(s_{kk} = 0)$ and the principal values are in the order of $S_1 \geq S_2 \geq S_3$ because $0 \leq \theta \leq \pi$. Substituting Eq. (8) into Eq. (5) gives:

$$\eta_A = \frac{\sigma_m}{\bar{\sigma}_A} = \frac{1}{3}\frac{\sigma_1 + \sigma_2 + \sigma_3}{|\sigma_1 - \sigma_3|\sqrt{-3Q}\left(\frac{1}{2}\right)^{\frac{1}{m}-1}\left\{\left[\sin\left(\frac{\pi - \theta_A}{3}\right)\right]^m + \left[\sin\left(\frac{\theta_A}{3}\right)\right]^m + \left[\sin\left(\frac{\theta_A + \pi}{3}\right)\right]^m\right\}^{\frac{1}{m}}} = \frac{1}{3}\frac{\sigma_1 + \sigma_2 + \sigma_3}{|\sigma_1 - \sigma_3|A} \tag{9}$$

It is worth to mention that the Yld91 criterion can reduce to special cases such as the Tresca (Tresca, 1864), the von Mises (Mises, 1913), the Hosford (Hosford, 1972), and the Hill's 48 (Hill, 1948) criteria. For example, when all components in the linear transformation operator $\mathbf{L}$ are set to unity, the IPE transformed tensor $\mathbf{s}$ reduces to the stress deviator tensor $\boldsymbol{\sigma}'$. In this case, the anisotropic stress triaxiality proposed can reduce to the isotropic stress triaxiality by setting the exponent of m to 2. In addition, the following explicit relation between the anisotropic parameters of the Yld91 and the Hill's 48 criteria can be obtained when the value of the exponent m is set to 2 (Prates et al., 2016):

$$F = \frac{2c_1^2 + c_1c_2 + c_1c_3 - c_2c_3}{6}, \quad L = \frac{3}{2}c_4^2$$
$$G = \frac{2c_2^2 + c_1c_2 + c_2c_3 - c_1c_3}{6}, \quad M = \frac{3}{2}c_5^2$$
$$H = \frac{2c_3^2 + c_1c_3 + c_2c_3 - c_1c_2}{6}, \quad N = \frac{3}{2}c_6^2 \tag{10}$$

The generalized anisotropic stress triaxiality based on the Yld91 criterion, therefore, has notable applicability for both isotropic and anisotropic cases.

2.2. Characterization of the stress states

It is straightforward to make an explicit relation between $(\sigma_1, \sigma_2, \sigma_3)$ and $(\eta_A, L_P, \bar{\sigma}_A)$ because the proposed anisotropic stress triaxiality and the Lode parameter are expressed by the principal stresses of the Cauchy stress tensor $\boldsymbol{\sigma}$ together with the fact

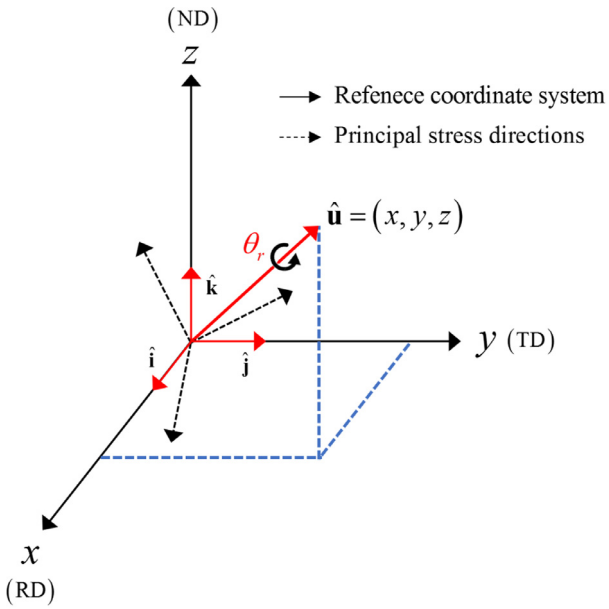

Fig. 1. Rotation axis and rotation angle for the coordinate transformation (after Park et al., 2017).

that the first invariant of the stress deviator tensor $\boldsymbol{\sigma}'$ is zero ($\sigma'_{kk} = 0$):

$$\begin{Bmatrix} \sigma_1 \\ \sigma_2 \\ \sigma_3 \end{Bmatrix} = \begin{Bmatrix} \sigma_m + \sigma'_1 \\ \sigma_m + \sigma'_2 \\ \sigma_m + \sigma'_3 \end{Bmatrix} = \begin{Bmatrix} \eta_A + \frac{3-L_P}{6A} \\ \eta_A + \frac{2L_P}{6A} \\ \eta_A - \frac{3+L_P}{6A} \end{Bmatrix} \bar{\sigma}_A$$

where

$$A = \sqrt{-3Q}\left(\frac{1}{2}\right)^{\frac{1}{m}-1}\left\{\left[\sin\left(\frac{\pi-\theta_A}{3}\right)\right]^m + \left[\sin\left(\frac{\theta_A}{3}\right)\right]^m + \left[\sin\left(\frac{\theta_A+\pi}{3}\right)\right]^m\right\}^{\frac{1}{m}} \tag{11}$$

Here, the principal stresses are in the order of $\sigma_1 \geq \sigma_2 \geq \sigma_3$. From the characterization of the stress states with the anisotropic stress triaxiality, it is possible to depict yield loci lying on three symmetric planes whose axes are coincident with the material symmetry axes as shown in Fig. 1. For example, when the plane stress condition is assumed as $\sigma_3 = 0$ concerning sheet metal forming application, the unit vector of the rotation axis is expressed as $\hat{\mathbf{u}} = x\hat{\mathbf{i}} + y\hat{\mathbf{j}} + z\hat{\mathbf{k}} = \hat{\mathbf{k}}$, such that the sub-functions in Eq. (2) reduce to:

$$f = 1 + \left(\frac{L_P-1}{2}\right)\cos^2\theta_S,\quad g = \left(\frac{L_P-1}{2}\right)\cos^2\theta_S - \left(\frac{1+L_P}{2}\right),$$
$$h = \left(\frac{1-L_P}{2}\right)\cos 2\theta_S\ n = \left(\frac{L_P-1}{4}\right)\sin 2\theta_S,\ l = m = 0 \tag{12}$$

In this case, the rotation angle θ_r strands for the loading direction θ_S as shown in Fig. 2.

The principal stresses lying on the normal surface of the sheet metal are then defined as:

$$\begin{Bmatrix} \sigma_1 \\ \sigma_2 \end{Bmatrix} = \frac{\bar{\sigma}_A}{\sqrt{-3Q'}\left(\frac{1}{2}\right)^{\frac{1}{m}-1}\left\{\left[\sin\left(\frac{\pi-\theta'_A}{3}\right)\right]^m + \left[\sin\left(\frac{\theta'_A}{3}\right)\right]^m + \left[\sin\left(\frac{\theta'_A+\pi}{3}\right)\right]^m\right\}^{\frac{1}{m}}} \times \begin{Bmatrix} 1 \\ \frac{1+L_P}{2} \end{Bmatrix}$$

where

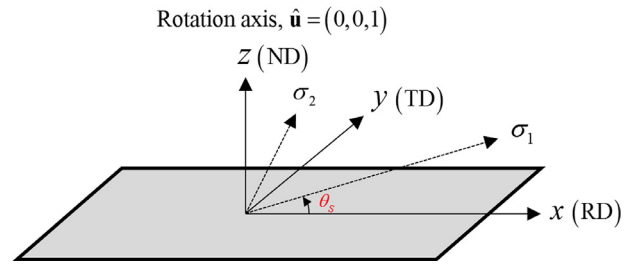

Fig. 2. Rotation axis and rotation angle defined for the application to sheet metal forming (after Park et al., 2017).

$$A' = \sqrt{-3Q'}\left(\frac{1}{2}\right)^{\frac{1}{m}-1}\left\{\left[\sin\left(\frac{\pi-\theta'_A}{3}\right)\right]^m + \left[\sin\left(\frac{\theta'_A}{3}\right)\right]^m + \left[\sin\left(\frac{\theta'_A+\pi}{3}\right)\right]^m\right\}^{\frac{1}{m}},\quad \theta'_A = \cos^{-1}\left(\frac{R'}{\sqrt{-Q'^3}}\right)$$

$$Q' = \frac{1}{9}\left(\frac{P_2}{3} - P_3\right)\left[P_1 + c_3\left(\frac{L_P-1}{2}\right)\cos 2\theta_S\right] - \frac{(P_1+P_2)^2}{27} - \frac{1}{12}c_6^2\sin^2 2\theta_S\left(\frac{L_P-1}{2}\right)^2$$

$$R' = \frac{P_1+P_2}{3}\left[\frac{1}{8}c_6^2\sin^2 2\theta_S\left(\frac{L_P-1}{2}\right)^2 - \frac{1}{18}(P_2-3P_3)(P_1+3P_3)\right]$$

$$P_1 = c_1\left[\left(\frac{L_P-1}{2}\right)\cos^2\theta_S + 1\right],\ P_2 = c_2\left[\left(\frac{1-L_P}{2}\right)\cos^2\theta_S + \frac{1+L_P}{2}\right],$$
$$P_3 = c_3\left(\frac{L_P-1}{6}\right)\cos 2\theta_S \tag{13}$$

Concerning the equi-biaxial stress state of $\sigma_1 = \sigma_2 = \sigma_b$ together with $\bar{\sigma}_A = \sigma_b$, A' in Eq. (13) becomes unity regardless of the values of the anisotropic parameters c_i ($i = 1, \ldots, 6$) and the exponent m as well as the loading direction θ_S. This makes the anisotropic stress triaxiality become a constant value of 2/3. The loss of the directionality on the equi-biaxial stress state can be reviewed from the definition of the anisotropic stress triaxiality as well. As an anisotropic indicator, the anisotropic stress triaxiality can be expressed as a quantity scaled from the isotropic stress triaxiality as follows:

$$\eta_A = \frac{\sigma_m}{\bar{\sigma}_A} = \frac{\sigma_m}{\bar{\sigma}_v}\frac{\bar{\sigma}_v}{\bar{\sigma}_A} = \eta_v\frac{\bar{\sigma}_v}{\bar{\sigma}_A} \tag{14}$$

where $\bar{\sigma}_v$ and $\bar{\sigma}_A$ represent the equivalent stresses of the von Mises isotropic yield criterion and the anisotropic yield criterion, respectively. A scaling factor, defined as the yield stress ratio of $\bar{\sigma}_v/\bar{\sigma}_A$, becomes unity when the equivalent stress of $\bar{\sigma}_A$ is set to the equi-biaxial yield stress σ_b, which leads to $\eta_A = \eta_v = 2/3$. Except for the equi-biaxial stress state, the scaling values depend on the Lode parameter L_P, the anisotropic parameters c_i ($i = 1, \ldots, 6$), and the exponent m:

$$\eta_A = \eta_v\frac{\sqrt{L_P^2+3}}{\sqrt{-3Q'}\left(\frac{1}{2}\right)^{\frac{1}{m}-2}\left\{\left[\sin\left(\frac{\pi-\theta'_A}{3}\right)\right]^m + \left[\sin\left(\frac{\theta'_A}{3}\right)\right]^m + \left[\sin\left(\frac{\theta'_A+\pi}{3}\right)\right]^m\right\}^{\frac{1}{m}}} \tag{15}$$

Fig. 3 shows the distribution of the scaling values in general stress states according to three loading directions of 0°, 45°, and 90° from the rolling direction of the sheet metal. Here, the parameters of the Yld91 criterion are calibrated using directional yield stresses of the DP980 1.2t steel sheet obtained from experiments by Park et al. (2017) and are summarized in Table 1. It is simply confirmed that the directionality of the equi-biaxial stress state ($L_P = 1$) vanishes for the reason that the scaling value becomes unity regardless of the loading direction as shown in Fig. 4.

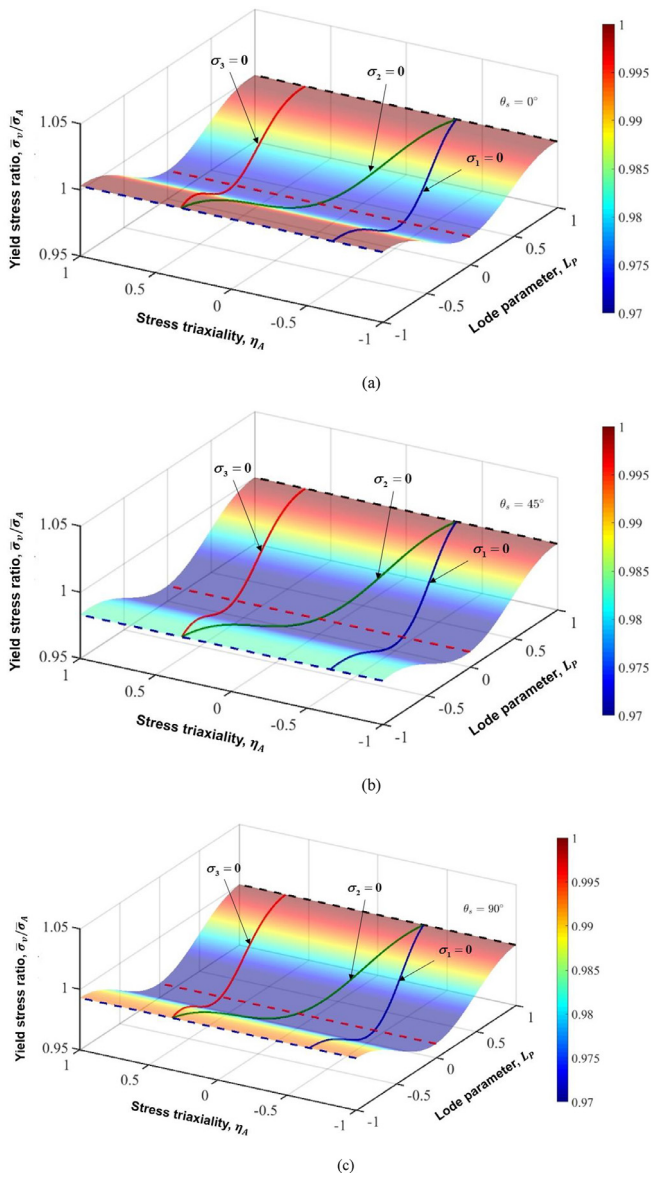

Fig. 3. Distribution of the scaling values over a wide range of stress states according to the three loading directions: (a) 0°; (b) 45°; (c) 90°.

Table 1
Anisotropic characteristic parameters of the Yld91 criterion determined by the normalized yield stresses.

c_1	c_2	c_3	c_4	c_5	c_6
1.010	0.990	1.004	1	1	1.023

2.3. Modeling of the anisotropic ductile fracture criterion considering the non-directionality of the equi-biaxial fracture strain

Dozens of anisotropic ductile fracture criteria have been proposed over the past decades with various hypotheses in both coupled and uncoupled approaches. For sheet metal forming application of advanced metals showing the low ductility, it is crucial to predict the onset of fracture accurately during complicated forming processes. In an attempt to guide the forming performance of advanced materials, the major and minor strains at the onset of fracture can be treated as a physical measure to evaluate the failure of advanced metal sheets. The series of those strain quantities constitutes the fracture forming limit diagram (FFLD) and can

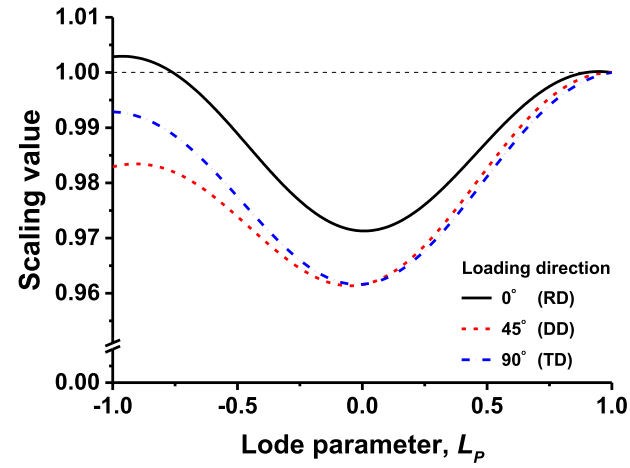

Fig. 4. Scaling values according to the Lode parameter at the three loading directions.

be obtained by either experiment or the theoretical model. In the present paper, we focus on the construction of the anisotropic failure model for an efficient application to the sheet metal forming industry.

As a one of the uncoupled approaches to demonstrate the effect of anisotropy on the fracture strain, a linear transformation can be considered in modeling the anisotropic ductile fracture criterion, which is discussed by Luo et al. (2012) and Gu and Mohr (2015) in detail. In this approach, the components of the linear transformation matrix are regarded as the parameters to be calibrated for the fracture criterion. The employment of the transformation approach therefore can give an increase in the model flexibility in evaluating the fracture strain at a certain loading state considering the loading direction. However, the enhancement of the model performance is not always guaranteed when employing the linear transformation because it also forces to increase in the non-linearity between the stress state and its corresponding fracture strain predicted from the fracture criterion. Each component in the transformation matrix plays a role as a factor to give more weight in certain loading states considering the influence of anisotropy on the fracture initiation. One of the limitations of this approach is that each weight factor is strongly related to the strain or stress component: therefore, the weight factors are determined by the least square scheme which will eventually result in the anisotropic fracture prediction in an average sense. To release the dependence of weight term on the stress or strain component, the components of the linear transformation matrix can be set as the value dependent on the loading direction. There remains, however, a difficulty to make the relationship of each component according to the loading direction in addition to a problem of the strong non-linearity among the model parameters. Meanwhile, in Park et al. (2017), a new attempt is made to deal with the general anisotropic FFLD for the application to advanced metals including aluminum alloys and it is also able to consider the non-directionality of the equi-biaxial stress state for the equivalent plastic strain while the directionality of the other stress states on the material orientation still holds. This anisotropic ductile fracture criterion, however, is limited to the material which conforms to the Hill's 48 criterion because it is defined by the anisotropic stress triaxiality based on the Hill's 48 criterion as follows:

$$\left(\frac{2\tau_{\max}}{\bar{\sigma}_H}\right)^{C_1}\left(\left\langle\frac{\sigma_1/\bar{\sigma}_H + C_O}{1 + C_O}\right\rangle\right)^{C_2}\bar{\varepsilon}_f^p \Rightarrow \left(\frac{1}{\sqrt{T}}\right)^{C_1} \times \left(\left\langle\frac{\eta_H + \frac{3-L_P}{6\sqrt{T}} + C_O}{1 + C_O}\right\rangle\right)^{C_2}\bar{\varepsilon}_f^p = C_3 \tag{16}$$

where $T = Ff^2 + Gg^2 + Hh^2 + 2\left(Ll^2 + Mm^2 + Nn^2\right)$

where C_O represents the stress sensitivity of the cut-off value for the stress triaxiality to microscopic structures, temperature, and so on. Under the plane stress condition, T reduces to T':

$$T' = F\left(\frac{1+L_P}{2}\cos^2\theta_S + \sin^2\theta_S\right)^2 + G\left(\cos^2\theta_S + \frac{1+L_P}{2}\sin^2\theta_S\right)^2 + \left(H\cos^2 2\theta_S + \frac{N}{2}\sin^2 2\theta_S\right)\left(\frac{1-L_P}{2}\right)^2 \quad (17)$$

To ensure the accuracy of the anisotropic fracture prediction, the parameters C_i in Eq. (16) can be considered as a function of the loading direction (Park et al., 2017):

$$C_i(\theta_S) = P_i\cos^4\theta_S + (4Q_i - R_i - P_i)\cos^2\theta_S\sin^2\theta_S + R_i\sin^4\theta_S, \quad i = 1, 2, 3 \quad (18)$$

where P_i, Q_i, and R_i denote the model parameters. Note that the directional dependence in Eq. (18) vanishes when the parameters of P_i, Q_i, and R_i are set to the same value. For the equi-biaxial stress state ($\eta_H = 2/3$, $L_P = 1$) under the plane stress condition ($\sigma_3 = 0$), Eq. (16) with Eq. (18) gives:

$$\left(\frac{1}{\sqrt{F+G}}\right)^{C_1(\theta_S)} \bar{\varepsilon}_f^b = C_3(\theta_S) \quad (19)$$

where $\bar{\varepsilon}_f^b$ represents the equivalent plastic strain at the onset of fracture under the equi-biaxial stress state. It is worth to note that $\bar{\varepsilon}_f^b$ becomes $C_3(\theta_S)$ only if the equivalent stress is set to the equi-biaxial yield stress, which leads to $F + G = 1$. Setting the model parameters of P_3, Q_3, and R_3 to the value of the equi-biaxial fracture strain subsequently, the non-directionality of the equi-biaxial fracture strain is eventually fulfilled. In a similar analogy to demonstrate the non-directionality of the equi-biaxial fracture strain, a new anisotropic ductile fracture criterion is proposed as:

$$\left(\frac{2\tau_{\max}}{\bar{\sigma}_A}\right)^{C_1(\theta_S)}\left(\left\langle\frac{\sigma_1/\bar{\sigma}_A + C_O}{1+C_O}\right\rangle\right)^{C_2(\theta_S)}\bar{\varepsilon}_f^p \Rightarrow \left(\frac{1}{A}\right)^{C_1(\theta_S)} \times \left(\left\langle\frac{\eta_A + \frac{3-L_P}{6A} + C_O}{1+C_O}\right\rangle\right)^{C_2(\theta_S)}\bar{\varepsilon}_f^p = C_3(\theta_S) \quad (20)$$

It can be simply verified that the proposed formula is able to consider the non-directionality of the equi-biaxial fracture strain from the fact that A becomes unity particularly when the material is subjected to the equi-biaxial stress state under the plane stress condition as discussed in Section 2.2. In addition, the model parameter $C_3(\theta_S)$ in Eq. (20) still has the same meaning of $\bar{\varepsilon}_f^b$ as before. In the viewpoint of the fracture prediction over a wide range of stress state, the fracture predictability of the fracture criterion proposed strongly depends on whether the non-directionality of the equi-biaxial strain holds. In general, the parameters of the facture criterion for advanced metals are calibrated by the quantities from typical loading states of the pure shear, the uniaxial tension, and the plane strain tension: those loading states play a significant role in determining the overall shape of the FFLD as well as a three-dimensional fracture envelope. If the non-directionality of the equi-biaxial fracture strain is considered in the calibration of the model parameters by eliminating the directional dependence of the parameter $C_3(\theta_S)$ through $P_3 = Q_3 = R_3 = \bar{\varepsilon}_f^b$, there may arise potential loss of the model predictability on the fracture strains for other loading states due to the inflexibility forced to the parameter $C_3(\theta_S) = \bar{\varepsilon}_f^b = C_3$. In an effort to overcome this drawback, a weight function is considered with Eq. (21):

$$w(\tilde{\mathbf{x}})\left(\frac{1}{A}\right)^{C_1(\theta_S)}\left(\left\langle\frac{\eta_A + \frac{3-L_P}{6A} + C_O}{1+C_O}\right\rangle\right)^{C_2(\theta_S)}\bar{\varepsilon}_f^p = C_3(\theta_S) \quad (21)$$

where $\tilde{\mathbf{x}}$ stands for the state variable vector. The weight function $w(\tilde{\mathbf{x}})$ is initially defined by the Cauchy stress tensor $\boldsymbol{\sigma}$ so as to deal with the general stress states. Since the Cauchy stress tensor is directly related to the anisotropic stress triaxiality, the Lode parameter, and the maximum principal stress direction, an equivalent form of the weight function can be expressed as $w(\eta_A, L_P, \theta_S)$. For the non-directionality of the equi-biaxial fracture strain, a value of the weight function is necessary to become unity under the equi-biaxial stress state. The weight function is thus simply proposed to have a form of:

$$w = \left(\frac{1}{\eta_A^2 + \frac{5}{9}}\right)^{C_4(\theta_S)} \quad \text{where } \eta_A = \frac{\sigma_m}{\bar{\sigma}_A} \quad (22)$$

With the adoption of the weight function, the final form of the uncoupled anisotropic ductile fracture criterion can be rewritten with the postulate of the plane stress condition for sheet metal forming application as follows:

$$\left(\frac{1}{A'}\right)^{C_1(\theta_S)}\left(\left\langle\frac{\eta_A + \frac{3-L_P}{6A'} + C_O}{1+C_O}\right\rangle\right)^{C_2(\theta_S)}\left(\frac{1}{\eta_A^2 + \frac{5}{9}}\right)^{C_4(\theta_S)}\bar{\varepsilon}_f^p = C_3 \quad (23)$$

Note that the proposed formula is valid only for the proportional loading. For the non-proportional loading, the fracture prediction is fulfilled by introducing a damage indicator D as a quantitative measure for ductility consumed at a material point. The range of the damage indicator traditionally runs from 0 to 1 and paths of damage growths can vary according to loading conditions and material properties. Recently, Cortese et al. (2016) introduced a non-linear damage accumulation law as:

$$D = \int_0^{\bar{\varepsilon}^p} \frac{m}{\left(\bar{\varepsilon}_f^p\right)^{q+1}}\left(\frac{\bar{\varepsilon}^p}{\bar{\varepsilon}_f^p}\right)^{\frac{m}{\left(\bar{\varepsilon}_f^p\right)^q}-1} d\bar{\varepsilon}^p \le 1 \quad (24)$$

where q and m are the material parameters which characterize the non-linearity in the damage accumulation and $\bar{\varepsilon}_f^p$ represents the equivalent plastic strain at the onset of fracture predicted from the fracture criterion. This non-linear damage accumulation law coincides with the one proposed by Xue (2007) and Papasidero et al. (2015) when $q = 0$. If $m = 1$ and $q = 0$, this approach reduces to the linear damage accumulation law. In aid of this damage accumulation law, we can evaluate the onset of fracture under non-proportional loading by performing a structural analysis via numerical simulation. Although it is very important to evaluate the performance of the new anisotropic ductile fracture criterion under the non-proportional loading, it is however not the scope of the present paper and will be further investigated later. The performance of the new anisotropic ductile fracture criterion will be discussed in Section 4 particularly for the proportional loading with a methodology to construct the anisotropic FFLD.

3. Prediction of the fracture forming severity of the DP980 1.2t steel sheet

The uncoupled anisotropic ductile fracture criterion proposed is applied to evaluate the fracture forming severity of the DP980 1.2t steel sheet under the proportional loading. In calibrating the parameters of the fracture criterion, the experimental results obtained by Park et al. (2017) were used, which are given in Table 2. In their research, three different types of tensile tests were conducted using various specimen geometries for a pure shear, a uniaxial tension, and a plane strain tension as shown in Fig. 5 to induce a certain deformation state at the material point where the onset of fracture is expected. Each specimen was fabricated along the loading directions of RD, DD, and TD so as to investigate the effect of material anisotropy on the fracture strain. The grayscale digital images were captured by the FASTCAM SA4 motion analysis

Table 2
Equivalent plastic strains at the onset of fracture according to the three loading direction (after Park et al., 2017).

Loading direction		Uniaxial tension case	Pure shear case	Plane strain tension case
0°(RD)	Test # 1	0.509	0.934	0.279
	Test # 2	0.545	0.962	0.313
	Test # 3	0.527	0.941	0.294
45°(DD)	Test # 1	0.640	0.783	0.255
	Test # 2	0.691	0.822	0.269
	Test # 3	0.672	0.806	0.262
90°(TD)	Test # 1	0.565	0.847	0.215
	Test # 2	0.603	0.887	0.246
	Test # 3	0.592	0.877	0.234

Table 3
Test conditions and results of the hydraulic bulge test of the DP980 1.2t steel sheet.

Specimen size [mm]	Punch speed [mm/s]	Clamping force [kN]	Equivalent plastic strain at the onset of fracture	
200 × 200	10	800	Test #1	0.616
			Test #2	0.723
			Test #3	0.669

Table 4
Yield stresses and *r*-values of the DP980 1.2t steel sheet.

Loading direction	Yield stress[a] [MPa]	*r*-value
0°(RD)	704	0.835
45°(DD)	690	1.101
90°(TD)	697	0.962
Equi-biaxial	702	1.041[b]

[a] 0.2% offset.
[b] $r_b = \varepsilon_{yy}/\varepsilon_{xx}$.

camera as a preparation for measuring the strain distribution on the surface of a specimen by means of the two-dimensional Digital Image Correlation (DIC) method using the commercial software of ARAMIS v6.3.0. The spatial resolution and frame rate used were around 0.02 mm/pixel and 20 frame/s, respectively. Experimental results showed that the strain path was maintained almost constantly during each test except for the uniaxial tension case: the strain path during the uniaxial tension test slightly changed after the necking as shown in Fig. 6. Since the change of strain paths was not severe during the tests, we simply assumed that the material is under the proportional loading condition before the fracture initiates. In this viewpoint, the equivalent plastic strain to fracture evaluated from the test can be regarded as the fracture strain corresponding the targeted loading condition induced by the specimen geometry, which can make possible to quantitatively evaluate the model performance in predicting the onset of fracture by comparing the fracture strains obtained from the tests with the ones predicted from the fracture criterion. In the present paper, hydraulic bulge tests were additionally carried out to obtain the equi-biaxial fracture strain with the three-dimensional DIC method. In the experiments, the equi-biaxial fracture strain was evaluated at the material point showing the maximum equivalent plastic strain just before the fracture initiation as shown in Fig. 7. Test conditions and results of the hydraulic bulge tests are listed in Table 3. The material properties of DP980 1.2t steel sheet and the parameters of the Hill's 48 criterion are briefly summarized in Tables 4 and 5, respectively.

3.1. Fracture envelope and fracture locus

The equivalent plastic strain to fracture obtained by Park et al. (2017) was evaluated by using the definition of the Hill's 48 equivalent plastic strain as a measure of the equivalent value. The equiv-

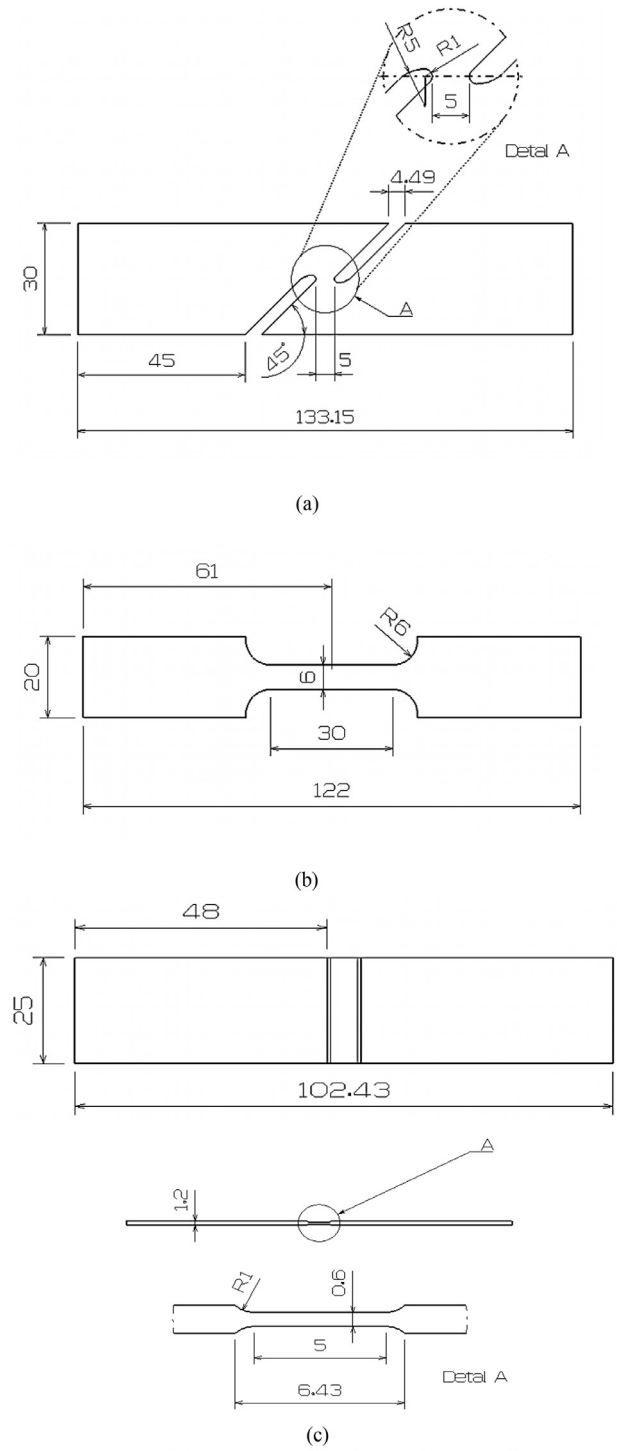

Fig. 5. Drawings of test specimens: (a) Pure shear specimen; (b) Dog-bone specimen; (c) Flat grooved specimen [mm] (after Park et al., 2017).

Table 5
Anisotropic characteristic parameters of the Hill's 48 criterion determined by the normalized yield stresses.

F	*G*	*H*	*L*	*M*	*N*
0.5100	0.4900	0.5044	1.5	1.5	1.5702

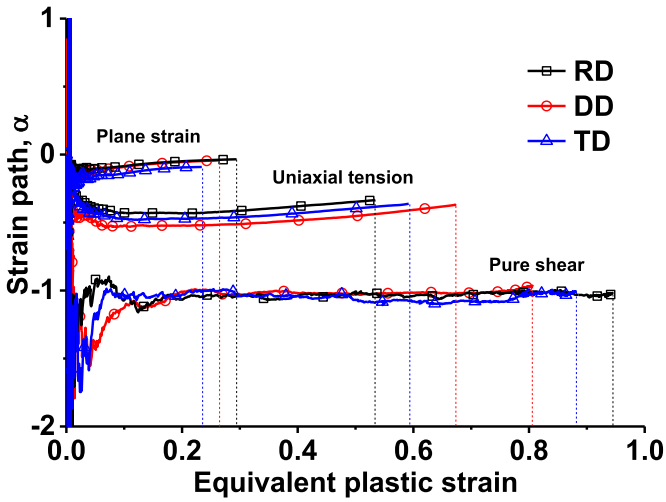

Fig. 6. Representative strain paths of the DP980 1.2t steel sheet according to the three sheet metal orientations (RD, DD, TD) and loading conditions (after Park et al., 2017).

Table 6
Parameters of the anisotropic ductile fracture criterion proposed.

i	P_i	Q_i	R_i	C_O
1	2.901	4.616	4.857	1/3
2	2.898	2.542	3.098	
3	0.669	0.669	0.669	
4	0.553	0.262	0.425	

alent quantities were obtained directly from the experiments by measuring the major and minor strain increments through the DIC analysis. As discussed in Section 2.1, the von Mises and the Hill's 48 criterion are the special cases of Yld91. Since the experimental results by Park et al. (2017) was used for the calibration of the parameters in the proposed fracture criterion, we adopted a reduced form of the proposed fracture criterion using the Hill's 48 criterion so as to achieve the consistency in the strain measurement, which also lies in a fact that the tested material obeys the Hill's 48 criterion. A special case of the proposed fracture criterion including the weight function can be expressed as follows:

$$\left(\frac{1}{\sqrt{T'}}\right)^{C_1(\theta_S)}\left(\left\langle\frac{\eta_H+\frac{3-L_P}{6\sqrt{T'}}+C_O}{1+C_O}\right\rangle\right)^{C_2(\theta_S)}\left(\frac{1}{\eta_H^2+\frac{5}{9}}\right)^{C_4(\theta_S)}\bar{\varepsilon}_f^p=C_3 \tag{25}$$

It is worth to note that the proposed fracture criterion and its reduced one defined by the Hill's 48 criterion exhibit the same performance in predicting the fracture strains used in the calibration of the model parameters due to its empirical characteristic resulting from the present form of each formula. It is, therefore, crucial to employ the measure of equivalent plastic strain which adequately demonstrates the deformation behavior of the tested material. It is also important to use its corresponding anisotropic stress triaxiality definition for the reliable fracture prediction, which should be further investigated more in detail via numerical analysis. The parameters of the above fracture criterion are optimized using the Nelder–Mead algorithm built in the MATLAB program with the use of the fracture strains averaged at each loading condition. The identified parameters are summarized in Table 6. As can be seen in Fig. 8, the fracture criterion proposed shows not only the characteristic of non-directionality of the equi-biaxial fracture strain but also the fracture predictability with great accuracy over a wide range of stress states according to the loading direction.

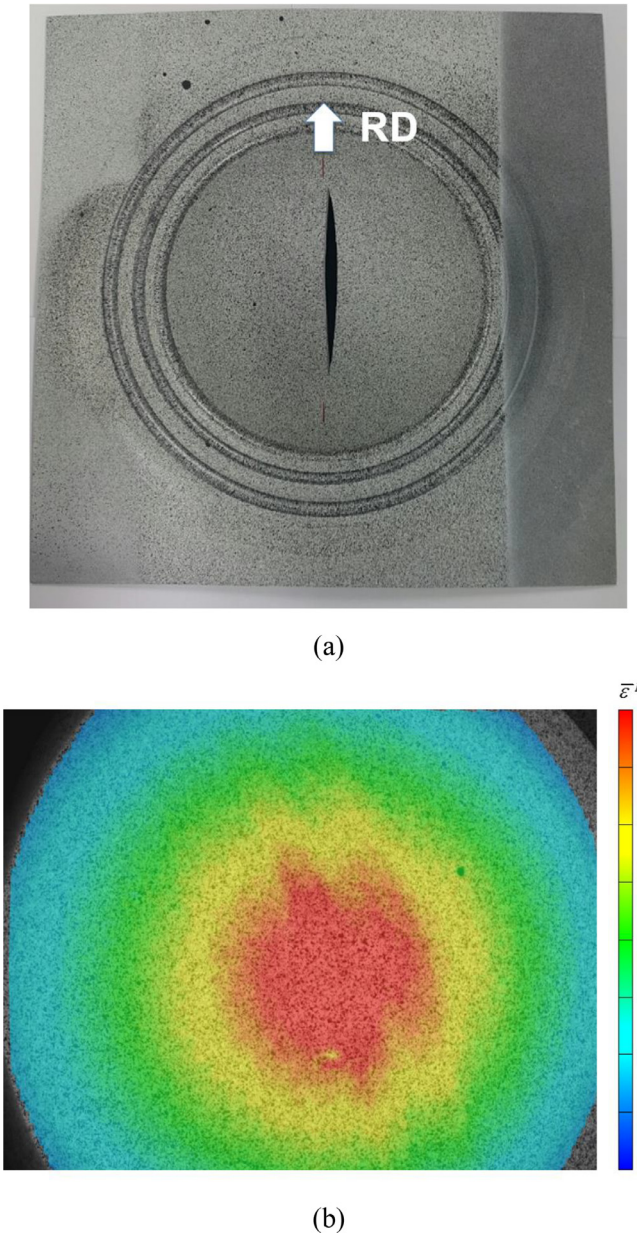

Fig. 7. Hydraulic bulge test result: (a) Fractured specimen; (b) Equivalent plastic strain distribution just before the fracture initiation.

For the confirmation of the model performance on the fracture prediction, fracture loci from the proposed fracture criterion are represented together with those from the anisotropic ductile fracture criterion without the weight function as shown in Fig. 9.

In this comparison, it is simply confirmed that the fracture predictability is significantly enhanced especially for the uniaxial tension condition including various loading states. This enhancement in the fracture predictability is closely associated with an increase in the number of the model parameters as well as an adequate description of the dependence of both the Lode parameter and the anisotropic stress triaxiality. The increase in the number of the model parameters, however, does not always ensure the enhancement of the model performance when the model has a high nonlinearity between a set of input variables and its corresponding output values. Meanwhile, the form of the fracture criterion proposed shows a clear linearity when it is reviewed in a logarithmic

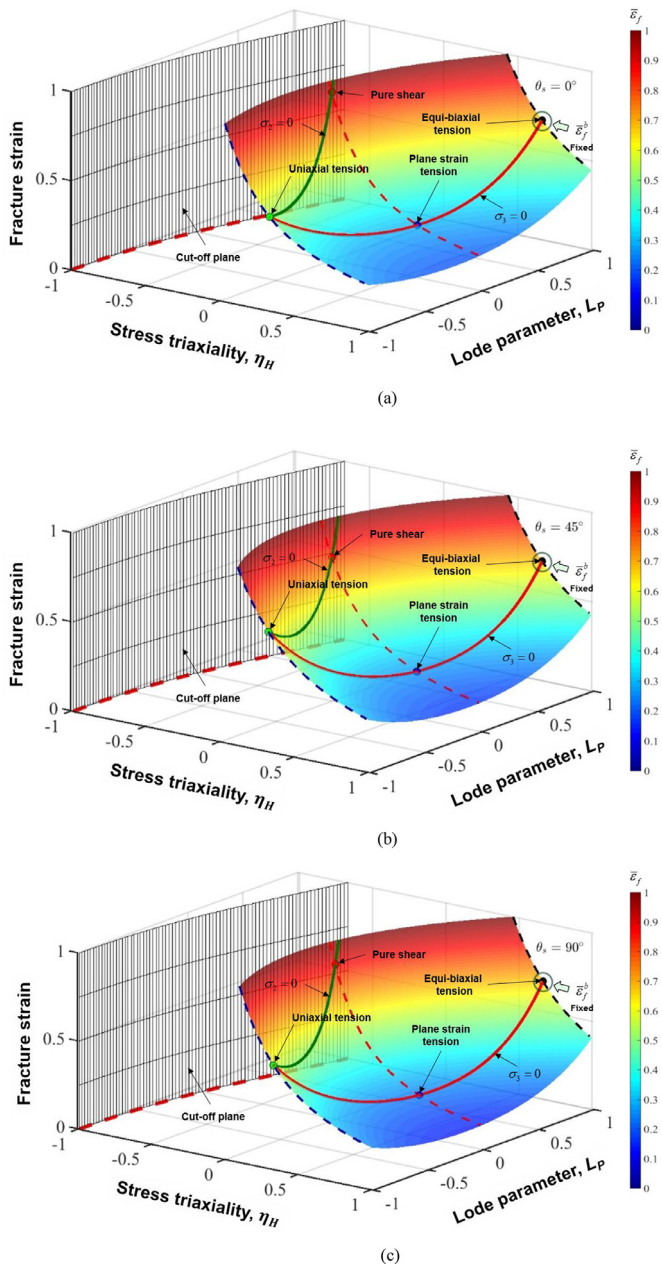

Fig. 8. Strain-based 3D fracture envelopes according to the three loading directions: (a) 0°; (b) 45°; (c) 90°.

form as follows:

$$C_1(\theta_S)\ln\left(\frac{1}{\sqrt{T'}}\right) + C_2(\theta_S)\ln\left(\left\langle\frac{\eta_H + \frac{3-L_P}{6\sqrt{T'}} + C_O}{1+C_O}\right\rangle\right) + C_4(\theta_S)\ln\left(\frac{1}{\eta_H^2 + \frac{5}{9}}\right) + \ln\bar{\varepsilon}_f^p = \ln C_3 \tag{26}$$

It is thus without a doubt that the enhancement of the model performance can be ensured in the present form of the fracture criterion proposed with the increase in the number of the model parameters.

3.2. Anisotropic fracture forming limit diagram

A theoretical transformation process is necessary to construct the FFLD from the uncoupled ductile fracture criterion. In general,

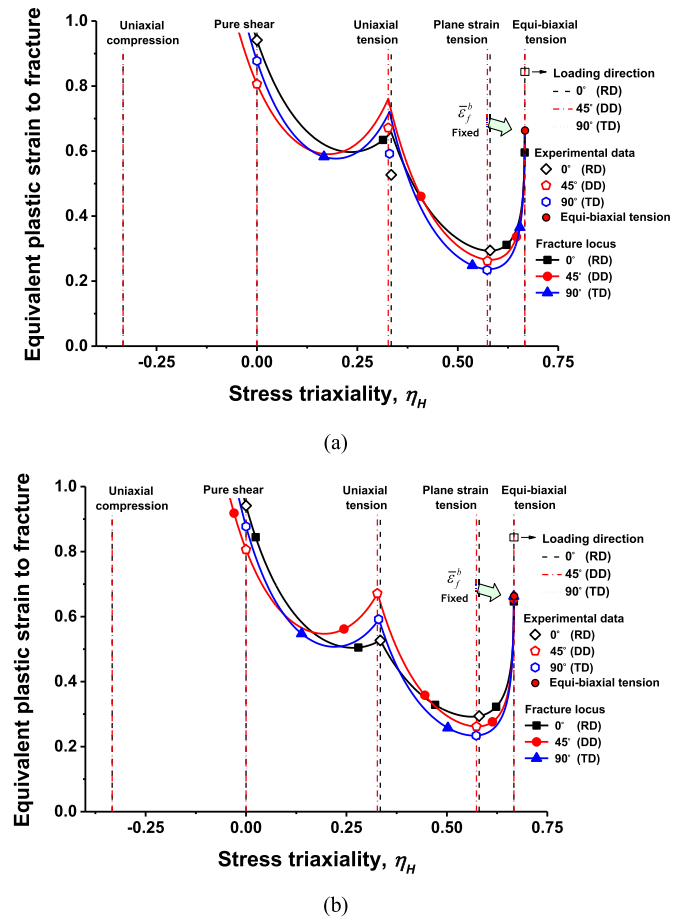

Fig. 9. Fracture loci of the DP980 1.2t steel sheet according to the loading direction: (a) Prediction from the anisotropic ductile fracture criterion without the weight function; (b) Prediction from a new anisotropic ductile fracture criterion with the weight function.

a transformation law is explicitly derived from the corresponding work-conjugate of the equivalent stress under the proportional loading. It is, however, not allowed to make an explicit form of the corresponding work-conjugate for non-quadratic yield criteria. As an alternative way to construct the FFLD, the explicit relation between the major and minor strains is rigorously derived in terms of the strain and stress paths based on the plastic work equivalence. It is worth to note that both methods to construct the FFLD are, in fact, equivalent from each other because those methods have the same base of the plastic work equivalence in their way of construction. The plastic work equivalence is defined as:

$$\dot{W} = \sigma_{ij}\dot{\varepsilon}_{ij}^p = \sigma_i\dot{\varepsilon}_i^p = \sigma_1\dot{\varepsilon}_1^p + \sigma_2\dot{\varepsilon}_2^p + \sigma_3\dot{\varepsilon}_3^p = \bar{\sigma}_A\dot{\bar{\varepsilon}}^p \tag{27}$$

Assuming the plane stress condition ($\sigma_3 = 0$) yields:

$$\sigma_1\dot{\varepsilon}_1^p\left(1 + \frac{\sigma_2}{\sigma_1}\frac{\dot{\varepsilon}_2^p}{\dot{\varepsilon}_1^p}\right) = \bar{\sigma}_A\dot{\bar{\varepsilon}}^p \rightarrow \dot{\varepsilon}_1^p = \frac{\bar{\sigma}_A}{\sigma_1}\frac{\dot{\bar{\varepsilon}}^p}{1+\alpha\beta}$$
$$\text{where } \alpha = \frac{\dot{\varepsilon}_2^p}{\dot{\varepsilon}_1^p},\ \beta = \frac{\sigma_2}{\sigma_1} \tag{28}$$

where α and β stand for the strain and stress paths. Under the proportional loading, the explicit relation between the major and minor strains can be derived as:

$$\int_0^{t_f}\dot{\varepsilon}_1^p dt = \int_0^{t_f}\frac{\bar{\sigma}_A}{\sigma_1}\frac{\dot{\bar{\varepsilon}}^p}{1+\alpha\beta}dt \Rightarrow \varepsilon_1^p = \frac{\bar{\sigma}_A}{\sigma_1}\frac{\bar{\varepsilon}_f^p}{1+\alpha\beta},$$
$$\varepsilon_2^p = \alpha\varepsilon_1^p = \frac{\partial Q(\boldsymbol{\sigma})/\partial\sigma_2}{\partial Q(\boldsymbol{\sigma})/\partial\sigma_1}\varepsilon_1^p \tag{29}$$

where t_f, $\bar{\varepsilon}_f^p$, and $Q(\boldsymbol{\sigma})$ represent time to fracture, the equivalent plastic strain at the onset of fracture predicted from the fracture criterion and a plastic potential, respectively. An explicit expression of $\bar{\sigma}_A/\sigma_i$ $(i = 1,\ 2,\ 3)$ can be obtained from Eq. (11) in terms of the anisotropic stress triaxiality and the Lode parameter. If the plane stress is assumed $(\sigma_i = 0,\ \text{with}\ i = 1,\ 2,\ 3)$ for sheet metal application, the relation between the anisotropic stress triaxiality and the Lode parameter is uniquely defined. This makes possible to explicitly express $\bar{\sigma}_A/\sigma_i$ $(i = 1,\ 2,\ 3)$ and the anisotropic ductile fracture criterion $\bar{\varepsilon}_f^p$ as a function of the Lode parameter only. Since the Lode parameter can be expressed by the stress ratio of the minor stress to the major stress under the plane stress condition, we can define the terms in Eq. (29) by the stress ratio except for α. Note that the strain ratio can be described by the stress ratio by associated flow rule. Following the transformation procedure introduced, an explicit relation between the major and minor strains is obtained in consideration of the general principal stress states as follows:

For intermediate stress triaxiality region (From the uniaxial tension to the equi-biaxial tension)

$$(\sigma_1 > 0, \sigma_2 > 0, \sigma_3 = 0)$$
$$\varepsilon_1 = \bar{\varepsilon}_f^p \frac{\bar{\sigma}_A}{\sigma_1} \frac{1}{1+\beta\alpha} = \bar{\varepsilon}_f^p A' \frac{1}{1+\beta\alpha},\ \varepsilon_2 = \alpha\varepsilon_1^p$$
$$\text{where}\ \beta = \frac{\sigma_2}{\sigma_1} = \frac{1+L_P}{2} \tag{30}$$

For low and negative stress triaxiality region (From the uniaxial compression to the uniaxial tension)

$$(\sigma_1 > 0, \sigma_2 = 0, \sigma_3 < 0)$$
$$\varepsilon_1 = \bar{\varepsilon}_f^p \frac{\bar{\sigma}_A}{\sigma_1} \frac{1}{1+\beta\alpha} = \bar{\varepsilon}_f^p \left(\frac{2A'}{1-L_P}\right) \frac{1}{1+\beta\alpha},\ \varepsilon_2 = \alpha\varepsilon_1^p$$
$$\text{where}\ \beta = \frac{\sigma_3}{\sigma_1} = -\frac{1+L_P}{1-L_P} \tag{31}$$

For negative stress triaxiality region (From the equi-biaxial compression to the uniaxial compression)

$$(\sigma_1 = 0, \sigma_2 < 0, \sigma_3 < 0)$$
$$\varepsilon_1 = \bar{\varepsilon}_f^p \frac{\bar{\sigma}_A}{\sigma_2} \frac{1}{1+\beta\alpha} = \bar{\varepsilon}_f^p \left(\frac{2A'}{-1+L_P}\right) \frac{1}{1+\beta\alpha},\ \varepsilon_2 = \alpha\varepsilon_1^p$$
$$\text{where}\ \beta = \frac{\sigma_3}{\sigma_2} = \frac{2}{1-L_P} \tag{32}$$

Consequently, the anisotropic FFLD can be constructed according to the loading direction when non-quadratic yield criterion is employed. Note that the overall shapes of the anisotropic FFLD as well as the fracture locus are strongly dependent on the exponent m which determines the curvature of non-quadratic yield function (Yld91). The change of yield surface curvature affects the value of anisotropic stress triaxiality, which eventually varies the shape of the fracture forming limit. Fig. 10 represents the influence of the exponent m on the yield surface and the fracture forming limits for the loading direction of 0°. Here, the parameters c_i of the Yld91 criterion are set to the values in Table 1.

For the reduced case of the anisotropic fracture criterion proposed as in Eq. (25), A' in Eqs. (30)–(32) reduces to $\sqrt{T'}$ and the relation between the strain and stress ratios is defined as follows:

$$\alpha = \frac{\left(2F\cos^2\theta_S\right)Q_1 + \left(2G\sin^2\theta_S\right)Q_2 - Q_3 - Q_4}{\left(2G\cos^2\theta_S\right)Q_2 + \left(2F\sin^2\theta_S\right)Q_1 + Q_3 + Q_4}$$

where

$$Q_1 = \beta\cos^2\theta_S + \sin^2\theta_S,\ \ Q_2 = \cos^2\theta_S + \beta\sin^2\theta_S,$$
$$Q_3 = H(1-\beta)(\cos 4\theta_S + 1),\ \ Q_4 = N\sin^2 2\theta_S(1-\beta) \tag{33}$$

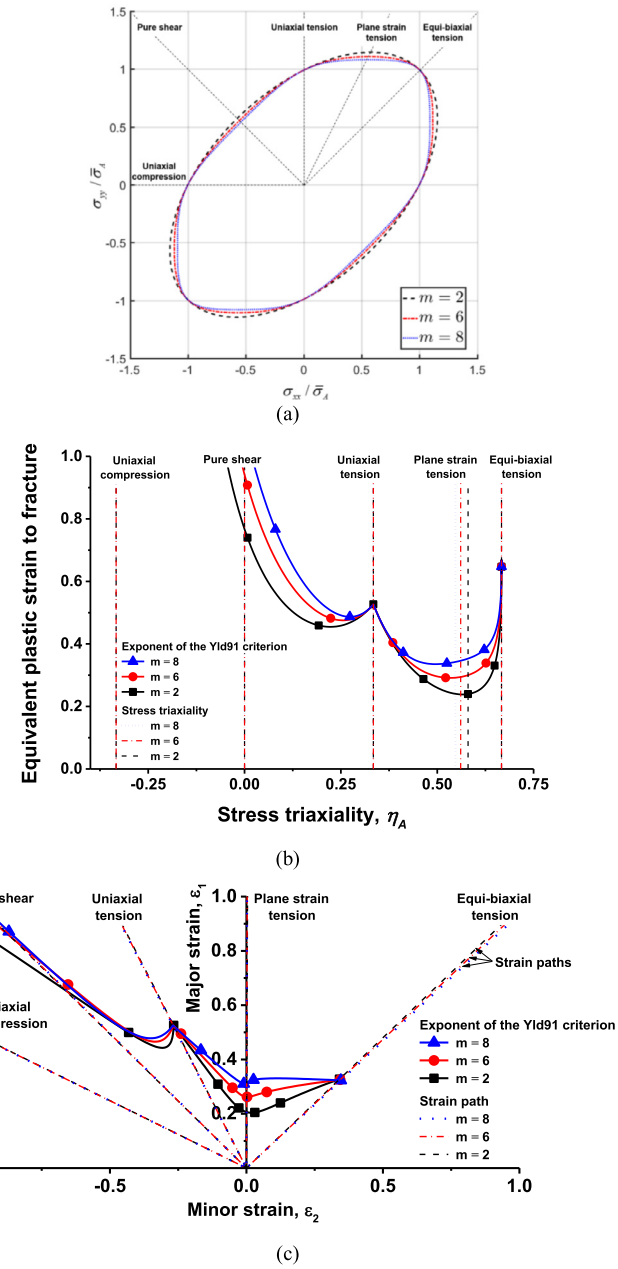

Fig. 10. Influence of the exponent m of the Yld91 criterion on the yield locus and the fracture forming limit: (a) Yield locus; (b) Fracture locus; (c) Fracture Forming Limit Diagram (FFLD).

The anisotropic FFLDs of the DP980 1.2t steel sheet are constructed through the transformation procedure from the fracture criterion and compared with those constructed from the anisotropic ductile fracture criterion without the weight function as shown in Fig. 11. It can be simply confirmed that the anisotropic FFLD constructed from the fracture criterion proposed shows a good performance in predicting the forming limit over a wide range of stress states. The strain paths, as shown in Fig. 9, represent the corresponding deformation modes considering the material anisotropy, which are theoretically predicted from Eq. (33) when the sheet metal is subjected to typical stress states with respect to the loading direction. A fracture forming limit envelope constructed is represented in Fig. 12.

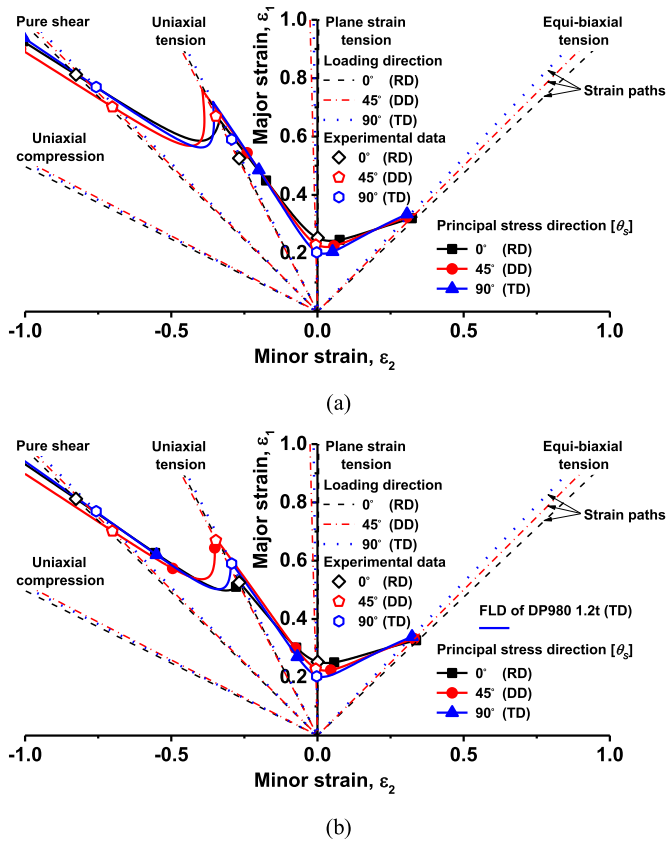

Fig. 11. Fracture Forming Limit Diagram (FFLD) of the DP980 1.2t steel sheet according to the loading direction: (a) Predicted from the anisotropic ductile fracture criterion without the weight function; (b) Predicted from a new anisotropic fracture criterion with the weight function.

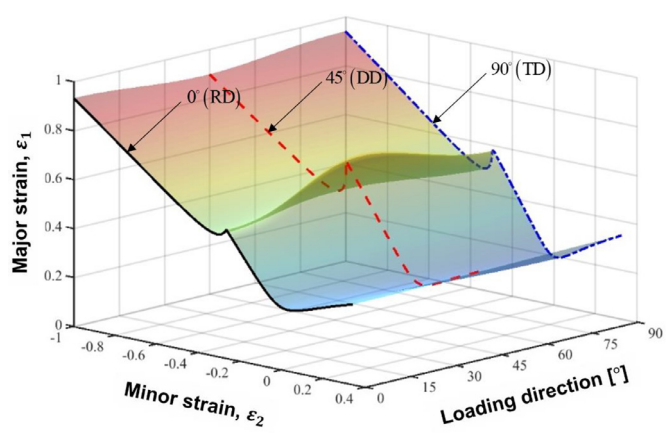

Fig. 12. Fracture forming limit envelope of the DP980 1.2t steel sheet.

4. Discussion

4.1. Fracture predictability at different loading directions

The improvement of the model performance on the fracture prediction was confirmed in Section 3 by comparing the fracture forming limit predicted from the proposed fracture criterion. This is quite promising because the parameters of the fracture criterion were calibrated directly from the experimental results. That is, more weight in the fracture prediction will be given to the stress states and the loading directions involved in the calibration of the model parameters. It is thus necessary to validate the predictability

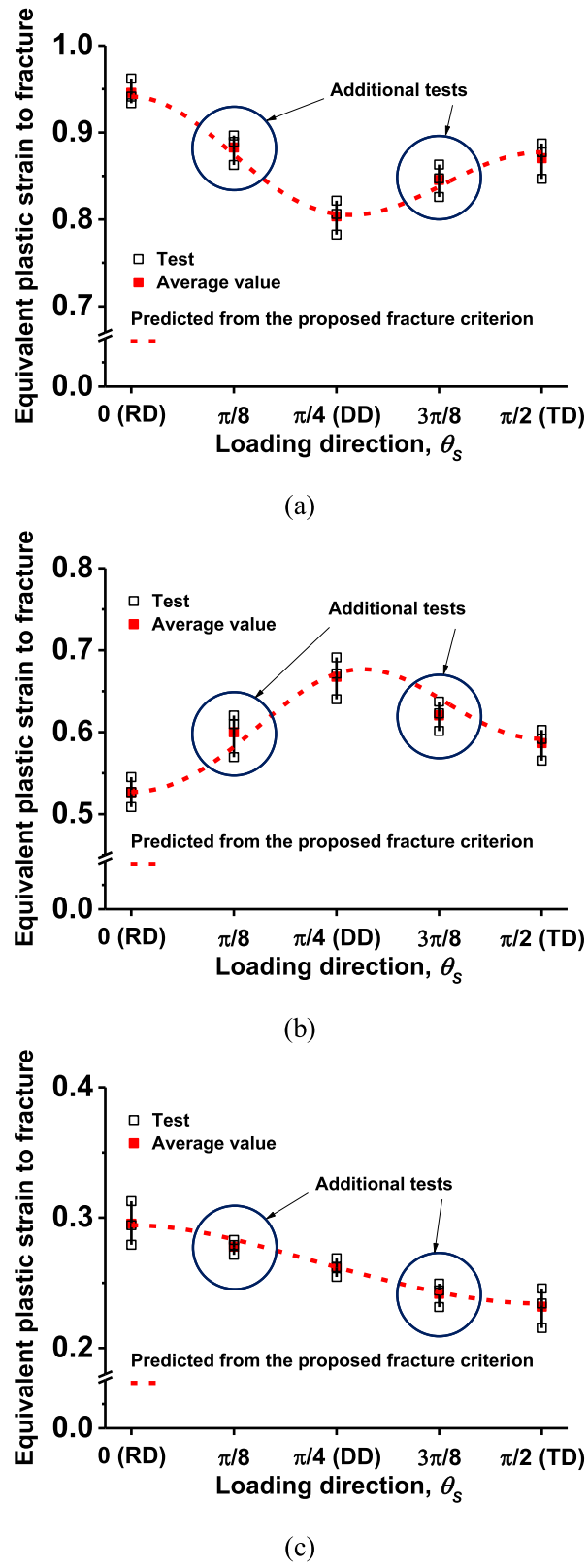

Fig. 13. Comparison of the fracture strains of the DP980 1.2t steel sheet obtained from the experiments with the ones predicted from the proposed fracture criterion: (a) Pure shear; (b) Uniaxial tension; (c) Plane strain tension.

Table 7
Equivalent plastic strains at the onset of fracture at loading directions of 22.5° and 67.5°.

Loading direction		Uniaxial tension case	Pure shear case	Plane strain tension case
22.5°	Test # 1	0.601	0.863	0.272
	Test # 2	0.570	0.897	0.279
	Test # 3	0.620	0.889	0.283
67.5°	Test # 1	0.602	0.847	0.249
	Test # 2	0.637	0.826	0.244
	Test # 3	0.623	0.863	0.231

of the fracture criterion with the experimental data not involved in the calibration of the model parameters. Additional experiments of the DP980 1.2t steel sheet were carried out accordingly with specimens fabricated along 22.5° and 67.5° to the rolling direction using the same material and the test conditions used for the experiments by Park et al. (2017). Three different types of specimen geometries were considered to induce typical stress states of the pure shear, the uniaxial tension, and the plane strain tension. Note that those specimen geometries were designed to have the same dimensions for each type considered in the previous experiments so as to disregard the possible influence of specimen geometry changes on the experimental data for the reliable comparison with the previous ones. Tensile tests were conducted three times to confirm the reproducibility from each test. With the Digital Image Correlation (DIC) method, equivalent plastic strains at the onset of fracture were measured at the material point showing the maximum equivalent plastic strain just before the onset of fracture. The obtained results are summarized in Table 7. It is clearly confirmed that the fracture criterion proposed is capable of predicting the onset of fracture over a wide range of stress state with great accuracy in comparison of the data evaluated from the experiments and it is also shown in Fig. 13.

5. Conclusions

A new uncoupled ductile fracture criterion is developed to provide a phenomenological model for considering non-directionality of the equi-biaxial fracture strain as well as the effect of anisotropy at the macroscopic level particularly for sheet metal forming application. After setting up anisotropic space through the anisotropic stress triaxiality based on the Yld91 criterion, a weight function is devised with the aim of enhancing the fracture predictability over a wide range of stress states in various loading directions. Since the Yld91 criterion can reduce to various yield criteria including the Hill's 48, Hosford, von Mises, and Tresca criteria, the generalized anisotropic stress triaxiality is capable of demonstrating the deformation behavior of various materials. This implies that the proposed fracture criterion has a considerable potential to deal with fracture behavior of various materials in the same explicit form in addition to the characteristic of non-directionality of the equi-biaxial fracture strain. In general, there exists the constitutive law to describe the yielding of material, which has influence on the shape of the fracture forming limit diagram. It is, therefore, necessary to have an in-depth understanding about which yield criterion is suitable for adequately demonstrating the material behavior during the sheet metal forming process. After figuring out one of the most suitable constitutive laws for the targeted material, it should be also applied to the fracture criterion by the anisotropic stress triaxiality defined by the constitutive law in consideration of the consistency in modeling of both fracture and yield criteria.

A transformation procedure is introduced to construct the anisotropic FFLD from the anisotropic fracture criterion with a non-quadratic yield criterion. The fracture criterion proposed is successfully applied to predict the forming severity of the DP980 1.2t steel sheet using experimental results by Park et al. (2017) and the hydraulic bulge test results conducted in the present work. Comparison of the experimental results with the ones predicted from the fracture criterion clearly reveals that the fracture criterion proposed has a considerable potential in describing the equivalent plastic strain at the onset of fracture over a wide range of stress states in consideration of the material anisotropy as well as non-directionality of the equi-biaxial fracture strain.

Appendix A. Generalization of anisotropic stress triaxiality based on the Yld2004-18p criterion

Barlat et al. (2005) proposed a generalization of the Hosford criterion for a pressure-independent material under general stress states with two linear transformations:

$$\phi\left(s_{\alpha\beta}\right) = \phi\left(\tilde{S}'_i, \tilde{S}''_j\right) = \sum_{i,j}^{1,3} \left|\tilde{S}'_i - \tilde{S}''_j\right|^m = 4\tilde{\sigma}_A^m \tag{A.1}$$

where m is a constant coefficient mainly associated with the crystal structure and the subscripts α and β stand for x, y, and z. Here, a reference frame (x, y, z) is assumed to be attached to the material symmetry axes as shown in Fig. 1. $\tilde{S}'_i$ and $\tilde{S}''_j$ are the principal values of the two transformed stress deviator $\tilde{\mathbf{s}}'$ and $\tilde{\mathbf{s}}''$ which can be written in a matrix form of

$$\tilde{\mathbf{s}} = \mathbf{Cs} = \begin{Bmatrix} \tilde{s}_{xx} \\ \tilde{s}_{yy} \\ \tilde{s}_{zz} \\ \tilde{s}_{yz} \\ \tilde{s}_{xz} \\ \tilde{s}_{xy} \end{Bmatrix} = \begin{bmatrix} 0 & -c_{12} & -c_{13} & 0 & 0 & 0 \\ -c_{21} & 0 & -c_{23} & 0 & 0 & 0 \\ -c_{31} & -c_{32} & 0 & 0 & 0 & 0 \\ 0 & 0 & 0 & c_{44} & 0 & 0 \\ 0 & 0 & 0 & 0 & c_{55} & 0 \\ 0 & 0 & 0 & 0 & 0 & c_{66} \end{bmatrix} \begin{Bmatrix} s_{xx} \\ s_{yy} \\ s_{zz} \\ s_{yz} \\ s_{xz} \\ s_{xy} \end{Bmatrix} \tag{A.2}$$

with the relevant symbols (prime and double prime) for each transformation: i.e., c'_{ij} for $\tilde{\mathbf{s}}'$ and c''_{ij} for $\tilde{\mathbf{s}}''$, respectively. The transformation tensor can also apply on the principal stress tensor of the Cauchy stress state as:

$$\tilde{\mathbf{s}} = \mathbf{Cs} = \mathbf{CT}\tilde{\sigma} = \mathbf{L}\tilde{\sigma} \Rightarrow \tilde{\mathbf{s}} = \mathbf{L}\tilde{\sigma} = \mathbf{LT}^*\tilde{\sigma}^{\mathrm{p}} = \mathbf{L}^*\tilde{\sigma}^{\mathrm{p}} \tag{A.3}$$

with

$$\mathbf{T} = \frac{1}{3}\begin{bmatrix} 2 & -1 & -1 & 0 & 0 & 0 \\ -1 & 2 & -1 & 0 & 0 & 0 \\ -1 & -1 & 2 & 0 & 0 & 0 \\ 0 & 0 & 0 & 3 & 0 & 0 \\ 0 & 0 & 0 & 0 & 3 & 0 \\ 0 & 0 & 0 & 0 & 0 & 3 \end{bmatrix},$$

$$\mathbf{T}^* = \begin{bmatrix} \left(tx^2+c\right)^2 & (txy+sz)^2 & (txz-sy)^2 \\ (txy-sz)^2 & \left(ty^2+c\right)^2 & (tyz+sx)^2 \\ (txz+sy)^2 & (tyz-sx)^2 & \left(tz^2+c\right)^2 \\ (txy-sz)(txz+sy) & \left(ty^2+c\right)(tyz-sx) & (tyz+sx)\left(tz^2+c\right) \\ \left(tx^2+c\right)(txz+sy) & (txy+sz)(tyz-sx) & (txz-sy)\left(tz^2+c\right) \\ \left(tx^2+c\right)(txy-sz) & (txy+sz)\left(ty^2+c\right) & (txz-sy)(tyz+sx) \end{bmatrix} \tag{A.4}$$

where $\tilde{\sigma}^{\mathrm{p}} = \{\sigma_1\ \sigma_2\ \sigma_3\}^T$, $t = 1 - \cos\theta_r$, $c = \cos\theta_r$, $s = \sin\theta_r$, $\hat{\mathbf{u}} = x\hat{\mathbf{i}} + y\hat{\mathbf{j}} + z\hat{\mathbf{k}}$ is the unit vector for the rotation axis and θ_r is the rotation angle as shown in Fig.1.

With the sub-functions of f, g, h, l, m, and n given in Eq. (2) whose forms are rigorously derived by the tensor transformation of the Cauchy stress tensor in aid of the Rodrigues' rotation formula,

Eq. (A.2) can be rewritten as:

$$\begin{Bmatrix} \tilde{s}_{xx} \\ \tilde{s}_{yy} \\ \tilde{s}_{zz} \\ \tilde{s}_{yz} \\ \tilde{s}_{xz} \\ \tilde{s}_{xy} \end{Bmatrix} = \frac{\sigma_1 - \sigma_3}{3} \begin{Bmatrix} c_{12}h + (c_{13} - c_{12})f + c_{13}(-g) \\ c_{21}(-h) + (c_{21} - c_{23})g + c_{23}f \\ (c_{32} - c_{31})h + c_{31}g + c_{32}(-f) \\ 3c_{44}l \\ 3c_{55}m \\ 3c_{66}n \end{Bmatrix} \tag{A.5}$$

The characteristic equation for $\tilde{\mathbf{s}}$ is defined as:

$$P(\tilde{S}_k) = \tilde{S}_k^3 - I_1\tilde{S}_k^2 - I_2\tilde{S}_k - I_3 = 0 \tag{A.6}$$

where I_1, I_2, and I_3 are the first, second and third invariants defined as:

$$\begin{aligned} I_1 &= \tilde{s}_{kk} = \frac{\tilde{s}_{xx} + \tilde{s}_{yy} + \tilde{s}_{zz}}{3} \\ I_2 &= \frac{\tilde{s}_{ij}\tilde{s}_{ji}}{2} = \frac{1}{3}I_1^2 - I_2 = \tilde{s}_{xx}\tilde{s}_{yy} + \tilde{s}_{yy}\tilde{s}_{zz} + \tilde{s}_{zz}\tilde{s}_{xx} - \tilde{s}_{xy}^2 - \tilde{s}_{yz}^2 - \tilde{s}_{zx}^2 \\ I_3 &= \frac{\tilde{s}_{ij}\tilde{s}_{jk}\tilde{s}_{kl}}{3} = \frac{2}{27}I_1^3 - \frac{1}{3}I_1I_2 + I_3 = \tilde{s}_{xx}\tilde{s}_{yy}\tilde{s}_{zz} + 2\tilde{s}_{xy}\tilde{s}_{yz}\tilde{s}_{zx} - \tilde{s}_{xx}\tilde{s}_{yz}^2 \\ &\quad - \tilde{s}_{yy}\tilde{s}_{zx}^2 - \tilde{s}_{zz}\tilde{s}_{xy}^2 \end{aligned} \tag{A.7}$$

Solving the above characteristic equation gives the principal values of $\tilde{\mathbf{s}}$ in terms of its invariants:

$$\begin{Bmatrix} \tilde{S}_1 \\ \tilde{S}_2 \\ \tilde{S}_3 \end{Bmatrix} = \frac{I_1}{3}\begin{Bmatrix} 1 \\ 1 \\ 1 \end{Bmatrix} + 2\sqrt{-Q}\begin{Bmatrix} \cos\left(\frac{\theta_A}{3}\right) \\ \cos\left(\frac{\theta_A - 2\pi}{3}\right) \\ \cos\left(\frac{\theta_A + 2\pi}{3}\right) \end{Bmatrix}$$

where

$$Q = \frac{3I_2 - I_1^2}{9},\ R = \frac{2I_1^3 - 9I_1I_2 + 27I_3}{54},\ \theta_A = \cos^{-1}\left(\frac{R}{\sqrt{-Q^3}}\right) \tag{A.8}$$

Because $0 \le \theta_A \le \pi$, the principal values are ordered, $\tilde{S}_1 \ge \tilde{S}_2 \ge \tilde{S}_3$. Substituting (A.5) into (A.7) yields:

$$I_1 = \frac{\sigma_1 - \sigma_3}{3}\begin{bmatrix} c_{12}h + (c_{13} - c_{12})f + c_{13}(-g) + c_{21}(-h) + (c_{21} - c_{23})g \\ + c_{23}f + c_{31}g + (c_{31} - c_{32})(-h) + c_{32}(-f) \end{bmatrix} \tag{A.9}$$

$$I_2 = (\sigma_1 - \sigma_3)^2 \begin{Bmatrix} \left[\frac{c_{12}h + (c_{13} - c_{12})f + c_{13}(-g)}{3}\right]\left[\frac{c_{21}(-h) + (c_{21} - c_{23})g + c_{13}f}{3}\right] \\ + \left[\frac{c_{21}(-h) + (c_{21} - c_{23})g + c_{13}f}{3}\right]\left[\frac{c_{31}g + (c_{31} - c_{32})(-h) + c_{32}(-f)}{3}\right] \\ + \left[\frac{c_{31}g + (c_{31} - c_{32})(-h) + c_{32}(-f)}{3}\right]\left[\frac{c_{12}h + (c_{13} - c_{12})f + c_{13}(-g)}{3}\right] \\ - c_{66}^2n^2 - c_{44}^2l^2 - c_{55}^2m^2 \end{Bmatrix} \tag{A.10}$$

$$I_3 = (\sigma_1 - \sigma_3)^3 \begin{Bmatrix} \left[\frac{c_{12}h + (c_{13} - c_{12})f + c_{13}(-g)}{3}\right]\left[\frac{c_{21}(-h) + (c_{21} - c_{23})g + c_{13}f}{3}\right]\left[\frac{c_{31}g + (c_{31} - c_{32})(-h) + c_{32}(-f)}{3}\right] \\ + 2c_{66}^2n^2c_{44}^2l^2c_{55}^2m^2 - \left[\frac{c_{12}h + (c_{13} - c_{12})f + c_{13}(-g)}{3}\right]c_{44}^2l^2 \\ - \left[\frac{c_{21}(-h) + (c_{21} - c_{23})g + c_{13}f}{3}\right]c_{55}^2m^2 - \left[\frac{c_{31}g + (c_{31} - c_{32})(-h) + c_{32}(-f)}{3}\right]c_{66}^2n^2 \end{Bmatrix} \tag{A.11}$$

From Eqs. (A.8)–(A.11), the sub-quantities of Q, R, and θ_A can be simply expressed as follows:

$$\begin{aligned} Q &= \frac{3I_2 - I_1^2}{9} = (\sigma_1 - \sigma_3)^2 A \\ R &= \frac{2I_1^3 - 9I_1I_2 + 27I_3}{54} = (\sigma_1 - \sigma_3)^3 B \\ \theta_A &= \cos^{-1}\left(\frac{R}{\sqrt{-Q^3}}\right) = \cos^{-1}\left[\frac{(\sigma_1 - \sigma_3)^3 B}{\sqrt{-(\sigma_1 - \sigma_3)^6 A^3}}\right] \\ &= \cos^{-1}\left(\frac{B}{\sqrt{-A^3}}\right) \end{aligned} \tag{A.12}$$

where A and B are the non-dimensional quantities associated with the normalized components of the rotation axis $\hat{u} = (x, y, z)$, the Lode parameter, and the rotation angle θ_r. With the transformation procedure introduced, the Yld 2004-18p criterion, defined by the principal values of the transformed stress deviators of $\tilde{\mathbf{s}}'$ and $\tilde{\mathbf{s}}''$, is expressed in terms of the principal stresses of the Cauchy stress tensor accordingly:

$$\phi = |\sigma_1 - \sigma_3|^m \sum_{i,j}^{1,3} \left| 2\sqrt{-A'}\cos\left[\frac{\theta'_A + 2\pi(i-2)}{3}\right] - 2\sqrt{-A''}\cos\left[\frac{\theta''_A + 2\pi(j-2)}{3}\right] + \frac{B' - B''}{3}\right|^m = 4\bar{\sigma}_A^m \tag{A.13}$$

with the symbols (prime and double prime) for each transformation of c'_{ij} and c''_{ij}. It is worth to mention that the equivalent stress of the Yld2004-18p criterion is unequivocally associated with a diameter of the Mohr's circle. This is sound from the point of view that the Yld2004-18p criterion starts from a framework of the maximum shear stress theory. The anisotropic stress triaxiality based on the Yld2004-18p criterion is defined by the principal stresses of the Cauchy stress tensor accordingly:

$$\eta_A = \frac{\sigma_m}{\bar{\sigma}_A} = \frac{\sigma_1 + \sigma_2 + \sigma_3}{3|\sigma_1 - \sigma_3|\left(\frac{1}{4}\right)^{\frac{1}{m}}\left\{\sum_{i,j}^{1,3}\left|2\sqrt{-A'}\cos\left[\frac{\theta'_A + 2\pi(i-2)}{3}\right] - 2\sqrt{-A''}\cos\left[\frac{\theta''_A + 2\pi(j-2)}{3}\right] + \frac{B' - B''}{3}\right|^m\right\}^{\frac{1}{m}}} = \frac{\sigma_1 + \sigma_2 + \sigma_3}{3|\sigma_1 - \sigma_3|A} \tag{A.14}$$

Since the Yld91 criterion is a particular case of the Yld2004-18p criterion, the anisotropic stress triaxiality based on Yld2004-18p criterion can reduce to the one defined by the Yld91 criterion particularly when the two linear transformations are equal: i.e. $\mathbf{C}' = \mathbf{C}''$ *or* $\mathbf{L}' = \mathbf{L}''$. The principal stresses are uniquely defined in terms of the anisotropic stress triaxiality, the Lode parameter, and the equivalent stress based on the Yld2004-18p criterion by applying the same analogy for the characterization of the stress states discussed in Section 2.2:

$$\begin{Bmatrix} \sigma_1 \\ \sigma_2 \\ \sigma_3 \end{Bmatrix} = \begin{Bmatrix} \sigma_m + \sigma'_1 \\ \sigma_m + \sigma'_2 \\ \sigma_m + \sigma'_3 \end{Bmatrix} = \begin{Bmatrix} \eta_A + \frac{3 - L_P}{6A} \\ \eta_A + \frac{2L_P}{6A} \\ \eta_A - \frac{3 + L_P}{6A} \end{Bmatrix}\bar{\sigma}_A$$

where

$$A = \left(\frac{1}{4}\right)^{\frac{1}{m}} \left\{ \sum_{i,j}^{1,3} \left| 2\sqrt{-A'} \cos\left[\frac{\theta'_A + 2\pi(i-2)}{3}\right] - 2\sqrt{-A''} \cos\left[\frac{\theta''_A + 2\pi(j-2)}{3}\right] + \frac{B' - B''}{3} \right|^m \right\}^{\frac{1}{m}} \quad (A.15)$$

References

Bao, Y.B., Wierzbicki, T., 2004. On fracture locus in the equivalent strain and stress triaxiality space. Int. J. Mech. Sci. 46 (1), 81–98.
Bai, Y., Wierzbicki, T., 2010. Application of extended Mohr–Coulomb criterion to ductile fracture. Int. J. Fract. 161, 1–20.
Barlat, F., Aretz, H., Yoon, J.W., Karabin, M.E., Brem, J.C., Dick, R.E., 2005. Linear transfomation-based anisotropic yield functions. Int. J. Plast. 21 (5), 1009–1039.
Barlat, F., Lege, D.J., Brem, J.C., 1991. A six-component yield function for anisotropic materials. Int. J. Plast. 7 (7), 693–712.
Børvik, T., Hopperstad, O.S., Pedersen, K.O., 2010. Quasi-brittle fracture during structural impact of AA7075-T651 aluminium plates. Int. J. Impact Eng. 37 (5), 537–551.
Budiansky, B., Hutchinson, J.W., Slutsky, S., 1982. Void Growth and Collapse in Viscous Solids. Pergamon Press, Oxford.
Brozzo, P., DeLuca, B., Rendina, R., 1972. A new method for the prediction of formability limits in metal sheets. In: Proceedings of the 7th Biennial Conference on Sheet Metal Forming and Formability, International Deep Drawing Research Group, Amsterdam, pp. 9–13.
Brünig, M., 2003a. An anisotropic ductile damage model based on irreversible thermodynamics. Int. J. Plast. 19 (10), 1679–1713.
Brünig, M., 2003b. Numerical analysis of anisotropic ductile continuum damage. Comput. Methods Appl. Mech. Eng. 192 (26–27), 2949–2976.
Brünig, M., 2006. Continuum framework for the rate-dependent behavior of anisotropic damaged ductile metals. Acta Mech 186 (1–4), 37–53.
Brünig, M., Albrecht, D., Gerke, S., 2011. Modeling of ductile damage and fracture behavior based on different micromechanisms. Int. J. Damage Mech. 20 (4), 558–577.
Chaboche, J.L., 1981. Continuous damage mechanics: a tool to describe phenomena before crack initiation. Nucl. Eng. Des. 64 (2), 233–247.
Chaboche, J.L., 1988a. Continuum damage mechanics: Part I – general concepts. J. Appl. Mech 55 (1), 59–64.
Chaboche, J.L., 1988b. Continuum damage mechanics: Part II – damage growth, crack initiation, and crack growth. J. Appl. Mech 55 (1), 65–72.
Clift, S.E., Hartley, P., Sturgess, C.E.N., Rowe, G.W., 1990. Fracture prediction in plastic deformation processes. Int. J. Mech. Sci. 32 (1), 1–17.
Cockcroft, M., Latham, D., 1968. Ductility and the workability of metals. J. Inst. Metals 96 (1), 33–39.
Cortese, L., Nalli, F., Rossi, M., 2016. A nonlinear model for ductile damage accumulation under multiaxial non-proportional loading conditions. Int. J. Plast. 85, 77–92.
Danas, K., Castaneda, P.P., 2012. Influence of the lode parameter and the stress triaxiality on the failure of elasto-plastic porous materials. Int. J. Solids Struct. 49 (11), 1325–1342.
Dunand, M., Mohr, D., 2010. Hybrid experimental-numerical analysis of basic ductile fracture experiments for sheet metals. Int. J. Solids Struct. 47 (9), 1130–1143.
Freudenthal, A.M., 1950. The Inelastic Behavior of Solids, first ed. Wiley, New York.
Gologanu, M., Leblond, J.B., Devaux, J., 1993. Approximate models for ductile metals containing non-spherical voids – case of axisymmetric prolate ellipsoidal cavities. J. Mech. Phys. Solids 41 (11), 1723–1754.
Goodwin, G.M., 1968. Application of Strain Analysis to Sheet Metal Forming Problems in the Press Shop SAE Technical Paper No. 680093.
Gu, G., Mohr, D., 2015. Anisotropic Hosford–Coulomb fracture initiation model: theory and application. Eng. Fract. Mech. 147, 480–497.
Gurson, A.L., 1977. Continuum theory of ductile rupture by void nucleation and growth. Part I: yield criteria and flow rules for porous ductile media. J. Eng. Mater. Technol. 99 (1), 2–15.
Hill, R., 1948. A theory of the yielding and plastic flow of anisotropic metals. Proc. R. Soc. Lond. A 193 (1033), 281–297.
Hill, R., 1952. On discontinuous plastic states, with special reference to localized necking in thin sheets. J. Mech. Phys. Solids 1, 19–30.
Hora, P., Tong, L., Reissner, J., 1996. A prediction method for ductile sheet metal failure in FE-simulation. In: Lee, J.K., Kinzel, G.L., Wagoner, R.H. (Eds.), Proceedings of the 3rd International Conference: NUMISHEET '96, Deadborn, pp. 252–256.
Hosford, W.F., 1972. A generalized isotropic yield criterion. J. Appl. Mech. 39 (2), 607–609.
Kachanov, L., 1958. Time of the rupture process under creep conditions. Isv. Akad. Nauk. SSR. Otd Tekh. Nauk. 8, 26–31.
Keeler, S.P., Backofen, W.A., 1964. Plastic instability and fracture in sheets stretched over rigid punches. ASM Trans. Quart. 56, 25–48.
Khan, A.S., Liu, H., 2012a. A new approach for ductile fracture prediction on Al 2024-T351 alloy. Int. J. Plast. 35, 1–12.
Khan, A.S., Liu, H., 2012b. Strain rate and temperature dependent fracture criteria for isotropic and anisotropic metals. Int. J. Plast. 37, 1–15.
Ko, Y.K., Lee, J.S., Huh, H., Kim, H.K., Park, S.H., 2007. Prediction of fracture in hub hole expanding process using a new ductile fracture criterion. J. Mater. Process. Technol. 187–188, 358–362.
Lemaitre, J., 1985. A continuous damage mechanics model for ductile fracture. J. Eng. Mater. Technol. 107 (1), 83–89.
Lemaitre, J., 1992. A Course on Damage Mechanics. Springer, Berlin.
Lemaitre, J., Demorat, R., Sauzay, M., 2000. Anisotropic damage law of evolution. Eur. J. Mech. A/Solids 19 (2), 187–208.
Lou, Y.S., Huh, H., Lim, S., Pack, K., 2012. New ductile fracture criterion for prediction of fracture forming limit diagrams of sheet metals. Int. J. Solids Struct. 49 (25), 3605–3615.
Lou, Y.S., Yoon, J.W., Huh, H., 2014. Modeling of shear ductile fracture considering a changeable cut-off value for stress triaxiality. Int. J. Plast. 54, 56–80.
Luo, M., Dunand, M., Mohr, D., 2012. Experiments and modeling of anisotropic aluminum extrusions under multi-axial loading – part II: ductile fracture. Int. J. Plast. 32, 36–58.
Marciniak, Z., Kuczynski, K., 1967. Limit strains in the processes of stretch forming sheet metal. Int. J. Mech. Sci. 9 (9), 609–620.
Mises, R.V., 1913. Mechanik der festen Koerper im plastisch-deformablen Zustand. Nachrichten von der Gesellschaft der Wissenschaften zu Göttingen. Mathematisch-Physikalische Klasse 4, 582–592.
Mohr, D., Marcadet, S.J., 2015. Micromechanically-motivated phenomenological Hosford–Coulomb model for predicting ductile fracture initiation at low stress triaxialites. Int. J. Solids Struct. 67, 40–55.
Nahshon, K., Hutchinson, J.W., 2008. Modification of the Gurson model for shear failure. Eur. J. Mech. A/Solids 27 (1), 1–17.
Nielsen, K.L., Tvergaard, V., 2010. Ductile shear failure or plug failure of spot welds modelled by modified Gurson model. Eng. Fract. Mech. 77 (7), 1031–1047.
Oh, S.I., Chen, C.C., Kobayashi, S., 1979. Ductile fracture in axisymmetric extrusion and drawing: Part 2: workability in extrusion and drawing. J. Eng. Ind. 101 (1), 36–44.
Oyane, M., Sato, T., Okimoto, K., Shima, S., 1980. Criteria for ductile fracture and their applications. J. Mech. Working Technol. 4 (1), 65–81.
Papasidero, J., Doquet, V., Mohr, D., 2015. Ductile fracture of aluminum 2014-T351 under proportional and non-proportional multi-axial loading: Bao–Wierzbicki results revisited. Int. J. Solids Struct. 69, 459–474.
Park, N., Huh, H., Nam, J.B., Jung, C.G., 2015. Anisotropy effect on the fracture model of DP980 sheets considering the loading path. Int. J. Automot. Technol. 16 (1), 73–81.
Park, N., Huh, H., Lim, S.J., Lou, Y., Kang, Y.S., Seo, M.H., 2017. Fracture-based forming limit criteria for anisotropic materials in sheet metal forming. Int. J. Plast. 96, 1–35.
Prates, P.A., Oliveira, M.C., Fernandes, J.V., 2016. Identification of material parameters for thin sheets from single biaxial tensile test using a sequential inverse identification strategy. Int. J. Mater. Form. 9 (4), 547–571.
Rodriguez, O., 1840. Des lois geometriques qui regissent les desplacements d'un systeme solide dans l'espace et de la variation des coordonnees provenant de deplacements consideres independamment des causes qui peuvent les produire. J. Math. Pure Appl 5, 380–440.
Saanouni, K., Chaboche, J.L., 2003. Computational damage mechanics. Application to metal forming. In: Milne, I., Ritchie, R.O., Karihaloo, B. (Eds.). Comprehensive Structural Integrity, 3. Elsevier, Oxford Chapter 7.
Stören, S., Rice, J.R., 1975. Localized necking in thin sheets. J. Mech. Phys. Solids 23 (6), 421–441.
Swift, H.W., 1952. Plastic instability under plane stress. J. Mech. Phys. Solids 1, 1–18.
Tresca, H., 1864. Memoire sur l'ecoulement des corps solides soumis a de fortes pressions. C. R. Acad. Sci. Paris 59, 754–758.
Tvergaard, V., Needleman, A., 1984. Analysis of the cup-cone fracture in a round tensile bar. Acta Metall 32 (1), 157–169.
Xue, L., 2007. Damage accumulation and fracture initiation in uncracked ductile solids subject to triaxial loading. Int. J. Solids Struct. 44 (16), 5163–5181.
Xue, L., 2008. Constitutive modeling of void shearing effect in ductile fracture of porous materials. Eng. Fract. Mech. 75 (11), 3343–3366.
Xue, L., Wierzbicki, T., 2008. Ductile fracture initiation and propagation modeling using damage plasticity theory. Eng. Fract. Mech. 75 (11), 3276–3293.
Zhu, X., Weimann, K., Chandra, A., 2001. A unified bifurcation analysis of sheet metal forming limits. J. Eng. Mater. Technol. 123 (3), 329–333.

Please cite this article as: N. Park et al., Anisotropic fracture forming limit diagram considering non-directionality of the equi-biaxial fracture strain, International Journal of Solids and Structures (2018), https://doi.org/10.1016/j.ijsolstr.2018.01.009